The anterior insular cortex→central amygdala glutamatergic pathway is critical to relapse after contingency management

Marco Venniro[1], **Daniele Caprioli**[2], **Michelle Zhang**[1], **Leslie R. Whitaker**[1], **Shiliang Zhang**[3], **Brandon L. Warren**[1], **Carlo Cifani**[4], **Nathan J. Marchant**[5], **Ofer Yizhar**[6], **Jennifer M. Bossert**[1], **Cristiano Chiamulera**[7], **Marisela Morales**[8], and **Yavin Shaham**[1]

[1]Behavioral Neuroscience Research Branch, Intramural Research Program, Baltimore NIDA, NIH, USA [2]Department of Physiology and Pharmacology "Vittorio Erspamer", Sapienza University of Rome, Rome, Italy [3]Electron Microscopy Core, Intramural Research Program, Baltimore NIDA, NIH, USA [4]University of Camerino School of Pharmacy, Pharmacology Unit, Camerino, Italy [5]Department of Anatomy and Neurosciences, VU University Medical Center, Amsterdam, The Netherlands [6]Department of Neurobiology, Weizmann Institute of Science, Rehovot, Israel [7]Department of Diagnostic & Public Health, University of Verona, Verona, Italy [8]Integrative Neuroscience Research Branch, Intramural Research Program, Baltimore NIDA, NIH, USA

Summary

Despite decades of research on neurobiological mechanisms of psychostimulant addiction, the only effective treatment for many addicts is contingency management, a behavioral treatment that uses alternative non-drug rewards to maintain abstinence. However, when contingency management is discontinued, most addicts relapse to drug use. The brain mechanisms underlying relapse after cessation of contingency management are largely unknown, and until recently, an animal model of this human condition did not exist. Here we used a novel rat model in which the availability of a mutually exclusive palatable food maintains prolonged voluntary abstinence from intravenous methamphetamine self-administration to demonstrate that activation of monosynaptic glutamatergic projections from anterior insular cortex to central amygdala is critical to relapse after cessation of contingency management. We identified the anterior insular cortex-to-central amygdala projection as a new addiction- and motivation-related projection and a potential target for relapse prevention.

The authors declare that they do not have any conflicts of interest (financial or otherwise) related to the text of the paper.

Introduction

Despite numerous basic research publications on brain mechanisms of cocaine and methamphetamine addiction using animal models (Dong and Nestler, 2014; Wolf, 2016), the only effective treatment for many psychostimulant addicts is contingency management (Higgins et al., 2004). In this behavioral method, the availability of non-drug rewards (e.g., monetary vouchers), given in exchange for being drug free, maintains prolonged abstinence in many psychostimulant addicts (Higgins et al., 2004). However, when contingency management is discontinued, most addicts relapse to drug use (Roll, 2007). The brain mechanisms underlying relapse after cessation of contingency management are largely unknown and until recently, an animal model of this human condition did not exist (Venniro et al., 2016).

We recently developed a choice-based rat model of relapse after voluntary abstinence (contingency management) (Caprioli et al., 2015a). In this model, we first train rats to self-administer palatable food (the alternative non-drug reward) and then to self-administer a drug for several weeks. We then assess relapse to drug seeking during early and late abstinence days in the absence of the alternative food reward. Between tests, we expose the rats to daily mutually exclusive choice sessions between the drug and food (Cantin et al., 2010; Caprioli et al., 2015b; Lenoir et al., 2007). Under these 'contingency management' conditions, like human addicts, male and female rats choose to abstain from methamphetamine or heroin when an alternative non-drug reward is available, but relapse to drug seeking when the alternative reward is removed (Caprioli et al., 2015a; Caprioli et al., 2017; Venniro et al., 2017). In our initial mechanistic study, we used the Daun02 inactivation procedure (Koya et al., 2009a) and found that dorsomedial striatum neuronal ensembles (identified by the neuronal activity marker Fos (Cruz et al., 2013; Morgan and Curran, 1991)) play a role in relapse to methamphetamine seeking after voluntary abstinence (Caprioli et al., 2017).

In the present study, we studied the role of central amygdala (CeA) and its afferent projections (Pitkanen, 2000) in relapse after voluntary abstinence. We focused on the CeA, because we and others previously found that neuronal activity in this brain region is critical for the time-dependent increases in cocaine, methamphetamine, and nicotine seeking after forced abstinence (incubation of drug craving) (Funk et al., 2016; Li et al., 2015b; Lu et al., 2005b; Xi et al., 2013). Additionally, pharmacological inhibition of CeA neuronal activity decreases reinstatement of cocaine seeking after extinction (Alleweireldt et al., 2006; Kruzich and See, 2001).

In Exp. 1, we determined whether relapse to methamphetamine seeking after voluntary abstinence is associated with increased Fos expression in CeA and the nearby basolateral amygdala (BLA). We also determined whether relapse and Fos expression are decreased by systemic injections of the selective dopamine Drd1 antagonist SCH39166 (Chipkin et al., 1988), because the effect of addictive drugs or drug-associated cues on Fos induction in different brain areas is dependent on activation of Drd1 (Ciccocioppo et al., 2001) and downstream extracellular signal-regulated kinase (ERK) (Girault et al., 2007; Lu et al., 2006). Additionally, we used RNAscope® *in situ* hybridization (Wang et al., 2012) to

double-label *Fos* with *Drd1* and *Drd2* to determine whether relapse after voluntary abstinence is associated with selective activation *Drd1*-expressing cells in CeA. Finally, recent studies demonstrated different roles of the CeA sub-nuclei—lateral (CeL) and medial (CeM)—in appetitive and aversive learned behaviors (Cai et al., 2014; Ciocchi et al., 2010; Haubensak et al., 2010; Kim et al., 2017; Li et al., 2013; Tovote et al., 2016). Therefore, we also determined whether relapse after voluntary abstinence is associated with selective activation *Drd1*-expressing cells in CeL and CeM.

Based on Exp. 1 results, in Exp. 2, we tested whether pharmacological blockade of CeA Drd1 with SCH39166 would mimic the systemic effect of the drug on relapse, as well as the pharmacological and anatomical specificity of this manipulation. In Exp. 3, our goal was to identify the afferent glutamatergic projection to CeA whose activation during the relapse test would precede CeA activation. For this purpose, we combined retrograde tracing via CeA injections of cholera toxin subunit B (CTb) (Luppi et al., 1990) with detection of Fos to determine relapse-associated activity in ventral and dorsal anterior insular cortex (AIV and AID, also called agranular anterior insular cortex (Shi and Cassell, 1998)), ventral medial prefrontal cortex (vmPFC), BLA, paraventricular nucleus of thalamus (PVT), and ventral subiculum (vSub) neurons projecting to CeA (Pitkanen, 2000). We found that relapse after voluntary abstinence was associated with selective activation of the AIV→CeA projection. Thus, in Exp. 4–5, we first reversibly inactivated the AIV with the GABA$_A$+GABA$_B$ receptor agonists (muscimol+baclofen) (McFarland and Kalivas, 2001) to determine whether AIV activity is critical to relapse after voluntary abstinence. Next, we used chemogenetics (Armbruster et al., 2007) to selectively inhibit the AIV→CeA projection (Mahler et al., 2014) during the relapse tests to determine the causal role of this projection in relapse after voluntary abstinence. Finally, in Exp. 6, we used electron microscopy and *ex vivo* brain slice electrophysiology to determine ultrastructural, functional, and biochemical properties of AIV inputs to CeA.

Based on the results of Exp. 1–6, we conclude that activation of *Drd1*-expressing cells in CeA by a monosynaptic glutamatergic projection from AIV, which primarily innervates the CeL, is critical to relapse to methamphetamine seeking after choice-based voluntary abstinence, a rat model of the human condition of relapse after cessation of contingency management.

Results

In the experiments described below (see STAR Methods for details), we first trained food-sated rats to press on the food-paired lever for a palatable food reward (5 pellets per reward delivery) for 6 days. We then trained them to lever press on the methamphetamine-paired lever for an intravenous methamphetamine reward (0.1 mg/kg/infusion) for 14 days (see timeline in Fig. 1A–4A). The two levers and the distinct food- and drug-associated cues were located on opposite sides of the self-administration chambers. Next, during the voluntary abstinence period (14 days), we gave the rats a mutually exclusive choice between the palatable food and methamphetamine (20 trials/day, 10 min inter-trial-interval); during the choice trials, the rats can earn either the palatable food or intravenous methamphetamine but not both (a contingency management manipulation) (Caprioli et al., 2015a; Caprioli et

al., 2017; Caprioli et al., 2015b; Venniro et al., 2017). On the next day, we tested the rats for relapse to methamphetamine seeking. During testing, the food-paired lever was not available (cessation of contingency management) and presses on the methamphetamine-paired lever (the operational measure of relapse to drug seeking in rat models (Shalev et al., 2002; Venniro et al., 2016)) resulted in contingent presentations of the light cue previously paired with drug infusions but not methamphetamine.

Food and methamphetamine training and voluntary abstinence phase (Exp. 1–5)

As in previous studies (Caprioli et al., 2015a; Venniro et al., 2017), non-food-restricted rats increased their palatable food and methamphetamine intake over time during the training phase and showed complete or almost complete suppression of methamphetamine self-administration during the choice sessions (voluntary abstinence) (see Fig. 1–4 and Table S1 for statistical reporting of these data).

Systemic Drd1 antagonist injections decreased relapse after voluntary abstinence and relapse-induced activation of CeA (Exp. 1)

We first determined whether relapse to methamphetamine seeking after voluntary abstinence is associated with increased Fos expression in CeA and BLA and whether systemic SCH39166 injections would decrease the relapse behavior and relapse-associated neuronal activity, as assessed by Fos. We found that relapse to methamphetamine seeking after voluntary abstinence was associated with increased Fos in CeA but not BLA, and that both relapse and relapse-induced Fos were decreased by systemic injections of SCH39166 (Fig. 1E–G). The analysis of lever presses during the 90-min relapse tests, which included the between-subjects factor of SCH39166 dose (0, 20 μg/kg) and the within-subjects factor of Lever (Active, Inactive) showed a significant main effect of SCH39166 dose [$F_{1,25}=13.5$, $p=0.001$] and Lever [$F_{1,25}=83.5$, $p<0.001$], and a significant interaction between the two factors [$F_{1,25}=13.5$, $p=0.001$]. The analysis of the Fos data, which included the between-subjects factors of Test condition (No test, Relapse test) and SCH39166 dose, and the within-subjects factor of Amygdala sub-region (CeA, BLA), showed a significant interaction between the three factors [$F_{1,39}=7.0$, $p=0.01$]. In a follow-up analysis, we quantified Fos within the CeL and CeM and found that relapse to methamphetamine seeking was associated with similar levels of Fos induction in the CeA sub-regions and that systemic SCH39166 decreased Fos in both CeL and CeM (Fig. S2B and Table S1). These results show that relapse after voluntary abstinence is associated with activation of both CeL and CeM.

Next, we determined the cell type of the *Fos*-positive neurons in CeA and BLA by co-labeling *Fos* with *Drd1* and *Drd2* receptors using RNAscope® *in situ* hybridization. We found that relapse to methamphetamine seeking was primarily associated with increased *Fos* in *Drd1*-expressing CeA neurons (Fig. 1J–L). During the 60-min relapse test, active lever presses were higher than inactive lever presses (Fig. 1H, Lever [$F_{1,5}=45.2$, $p<0.001$]). The analysis of *Fos*, which included the between-subjects factor of Test condition (No test, Relapse test) and the within-subjects factor of Amygdala sub-region, showed a significant interaction between the two factors [$F_{1,8}=14.5$, $p=0.005$] (Fig. 1J); these *mRNA* data confirm that relapse to methamphetamine seeking is associated with selective activation of CeA but not BLA. The analysis of dopamine receptor expression showed a significant

interaction between Amygdala sub-region and Cell type [$F_{1,8}=38.5$, $p<0.001$] (Fig. 1K) due to higher expression of *Drd1* in BLA and *Drd2* in CeA. The analysis of double-labeled cells showed significant main effects of Cell type [$F_{1,8}=16.1$, p=0.004] and Amygdala sub-region [$F_{1,8}=38.6$, $p<0.001$] (Fig. 1L) due to higher *Fos* co-labeling in *Drd1* neurons than in *Drd2* neurons and overall higher *Fos* in CeA than in BLA (see above). We also analyzed the expression of *Fos*, *Drd1*, *Drd2* and double-labeled cells in CeL and CeM. We found that relapse to methamphetamine seeking is associated with activation of *Drd1*-expressing neurons in both CeL and CeM (Fig. S2C–F and Table S1).

CeA Drd1 antagonist injections decreased relapse after voluntary abstinence (Exp. 2)

Based on the results of Exp. 1, we determined in Exp. 2 whether CeA SCH39166 injections would mimic the systemic effect of the drug on relapse after voluntary abstinence. We also determined the anatomical and pharmacological specificity of this effect by injecting SCH39166 into the BLA and the selective Drd2 antagonist raclopride (a drug that does not inhibit Fos (Robertson and Jian, 1995)) into the CeA.

We found that SCH39166 injections into CeA, but not BLA, decreased relapse after voluntary abstinence (Fig. 2E–F). For CeA, the analysis of lever presses during the 120-min relapse tests, which included the between-subjects factor of SCH39166 dose (0, 0.5, 1.0 μg/ side) and the within-subjects factor of Lever showed a significant effect of SCH39166 dose [$F_{2,21}=8.4$, $p=0.002$] and Lever [$F_{1,21}=158.4$, $p<0.001$], and a significant interaction between the two factors [$F_{2,21}=8.2$, $p=0.002$]. For BLA, the analysis showed no effect of SCH39166 dose (0, 1.0 μg/side) [$p=0.94$]. We also found that raclopride injections into the CeA had no effect on relapse (Raclopride dose, 0, 0.5, 1.0 μg/side, [$p=0.99$]) (Fig. 2G).

Relapse after voluntary abstinence is associated with selective activation of the AIV→CeA projection (Exp. 3)

In Exp. 1–2, we identified a critical role of CeA activity in relapse after voluntary abstinence. In Exp. 3, we used the retrograde tracer CTb (injected into CeA) in combination with Fos to identify afferent projection regions to CeA whose activation would lead to activation of CeA during the relapse test. We found that relapse after voluntary abstinence was associated with selective activation of the AIV (anterior insular cortex ventral)→CeA projection but not the CeA afferent projections from vmPFC, AID (anterior insular cortex dorsal), BLA, PVT, or vSub (Fig. 3E–F & Fig. S4A–G). Relapse after voluntary abstinence was also associated with projection-independent Fos induction in AIV, AID, vmPFC, and PVT, but not BLA and vSub (Fig. S4A–G). We also analyzed Fos, CTb, and Fos+CTb expression throughout the AI and found that neurons expressing Fos, CTb, or dual Fos+CTb labeling were concentrated in the anterior portion of the insula and diminished along the posterior axis (Fig. 3F & Fig. S5A–C). [Note: we also analyzed Fos and double-labeling of Fos+CTb in substania nigra (no CTb labeling was observed in ventral tegmental area) and found that relapse after voluntary abstinence was not associated with activation of substania nigra neurons or activation of the substantia nigra projection to CeA (data not shown)].

During the 90-min relapse test, active lever presses were higher than inactive lever presses (Fig. 3E; Lever [$\chi^2(1)=4.0$, $p=0.046$]). The analysis of Fos alone, which included the

between-subjects factors of Test condition (No test, Relapse test), showed a significant main effect of Test condition in AIV [U=0, p=0.02], vmPFC [U=1, p=0.04], AID [U=0.0, p=0.02], and PVT [U=1.0, p=0.04]. For CTb+Fos double-labeling, the analysis, which included the between-subjects factor of Test condition showed a significant main effect of Test condition in AIV [U=0, p=0.02] but not in the other brain regions (p-values>0.05)

Inhibition of neuronal activity in AIV and AIV→CeA projection decreased relapse after voluntary abstinence (Exp. 4–5)

In Exp. 3, we found that relapse after voluntary abstinence is associated with activation of the AIV→CeA projection. Based on these results, we first used a traditional reversible inactivation (muscimol+baclofen) method (McFarland and Kalivas, 2001) to determine the causal role of AIV in relapse after voluntary abstinence (Exp. 4). Next, we used a DREADD-based projection selective inhibition method (Mahler et al., 2014) to determine the causal role of the AIV→CeA projection in relapse after voluntary abstinence (Exp. 5). We found that both experimental manipulations decreased relapse to methamphetamine seeking after voluntary abstinence, and that projection-specific inhibition also led to decreased CeA activity, as assessed by Fos (Fig. 3G & Fig. 4E).

AIV inactivation with muscimol+baclofen (M+B)—The statistical analysis of lever presses during the 120-min tests, which included the between-subjects factor of M+B dose and the within-subjects factor of Lever, showed a significant main effect of M+B dose [$F_{1,20}$=9.1, p=0.007] and Lever [$F_{1,20}$=102.1, p<0.001], and a significant interaction between the two factors [$F_{1,20}$=13.0, p=0.002]. In contrast, M+B injections into the nearby OFC (anatomical control) had no effect on relapse [p=0.77 for M+B dose)] (Fig. 3H).

AIV→CeA projection-specific inhibition with DREADD—The statistical analysis of lever presses during the 90-min tests, which included the between-subjects factor of CNO dose (0, 1.0 mM) and the within-subjects factor of Lever, showed a significant main effect of CNO dose [$F_{1,28}$=7.3, p=0.01] and Lever [$F_{1,28}$=127.3, p<0.001], and a significant interaction between the two factors [$F_{1,28}$=7.5, p=0.01] (Fig. 4E). In contrast, CNO injections into CeA without viral infection had no effect on relapse [p=0.89 for CNO dose] (Fig. 4F). Analysis of Fos induced during the 90-min relapse test showed that CNO decreased Fos expression in the hM4Di-injected rats [CNO dose: $F_{1,28}$=28.4, p=0.001] (Fig. 4E) but not in the control groups not injected with hM4Di [$F_{1,15}$=0.0, p=0.91] (Fig. 4F). Additionally, bath application of CNO in CeA neurons adjacent to mCherry+ AIV terminals reduced the magnitude of evoked EPSC [CNO dose x mCherry expression (+,-) interaction: $F_{1,14}$=6.7, p=0.02] (n=9 mCherry$^+$ and 7 mCherry$^-$ cells) (Fig. 5A), and decreased frequency of spontaneous synaptic events [CNO dose x mCherry expression: $F_{1,14}$= 9.6, p=0.008] (Fig. 5B). In contrast, CNO application had no effect on spontaneous event amplitude [CNO dose x mCherry expression: $F_{1,14}$=0.03, p=0.86] (Fig. 5B) (n=8 mCherry$^+$ and 8 mCherry$^-$ cells).

Glutamate neurons from AIV establish monosynaptic asymmetric (putative excitatory) synapses on CeA neurons (Exp. 6)

To determine the anatomical characteristics of the projection from AIV to CeA, we tagged AIV neurons and their axons by AIV injections of an adeno-associated virus (AAV) encoding mCherry under the control of the human Synapsin (hSyn) promoter. We then used double immunofluorescence and confocal microscopy to identify and count CeL and CeM terminal-like puncta that co-express mCherry and vGluT1 (Fig. 6A). The results of our neuronal counting indicate that AIV vGluT1-expressing neurons preferentially innervate the CeL sub-region of the CeA. By immunoelectron microscopy, we determined the ultrastructural properties of CeA mCherry-vGluT1 terminal-like puncta. We found that these puncta correspond to axon terminals that establish asymmetric (excitatory-type) synapses on dendrites (Fig. 6A). These ultrastructural findings indicate that vGluT1 neurons from the AIV establish glutamatergic excitatory synapses preferentially on CeL neurons.

Finally, to determine whether the glutamatergic projection from AIV is monosynaptic, we injected AAV-ChR2-eYFP into AIV under the control of a CaMKII promoter (Fig. 6B). Using *ex vivo* brain slice electrophysiology, we recorded light-evoked excitatory postsynaptic currents in CeA neurons in contact with eYFP-expressing terminals. We used bath application of the sodium channel blocker tetrodotoxin (TTX; 1 μM) to prevent action potential-induced activity within the CeA. We found no effect of TTX on the amplitude of the light-evoked currents, indicating that the projection is monosynaptic [p=0.53] (Fig. 6B).

Discussion

We studied the role of CeA and its afferent projections in relapse to methamphetamine seeking after voluntary abstinence, an animal model of relapse after cessation of contingency management. We report six main findings. First, relapse after voluntary abstinence was associated with increased Fos (a neuronal activity marker) in CeA *Drd1*-expressing neurons, with similar pattern of activation in CeL and CeM. Second, systemic injections of the Drd1 antagonist SCH39166 decreased both relapse and relapse-associated increases in CeA activity. Third, the systemic effect of SCH39166 was mimicked by CeA drug injections; in contrast, CeA injections of raclopride (a Drd2 antagonist) or BLA injections of SCH39166 were ineffective, demonstrating anatomical and pharmacological specificity. Fourth, relapse after voluntary abstinence was associated with selective activation of the AIV→CeA projection. Fifth, reversible inactivation of the AIV and, more importantly, chemogenetic inhibition of the AIV→CeA projection decreased relapse; inhibition of the AIV→CeA projection also decreased CeA Fos. Finally, electron microscopy and electrophysiology data showed that AIV vGluT1-expressing projection-neurons preferentially innervate the CeL sub-region of CeA and form monosynaptic glutamatergic asymmetric synapses on CeA cells. Our results demonstrate a critical role of Drd1-mediated neuronal activity in CeA that is controlled by AIV→CeA glutamatergic projections in relapse to methamphetamine seeking after voluntary abstinence.

Role of central amygdala

We found that relapse after voluntary abstinence was associated with selective activation of the CeL and CeM sub-nuclei of CeA, but not BLA, and that CeA but not BLA SCH39166 injections decreased relapse. This pattern of results is consistent with previous results from incubation of craving studies on the role of CeA but not BLA in 'incubated' cocaine, methamphetamine, or nicotine seeking after forced abstinence (Funk et al., 2016; Li et al., 2015b; Lu et al., 2005b; Lu et al., 2007; Xi et al., 2013). The present and previous results indicate that CeA activity plays a critical role in drug seeking after prolonged abstinence, independent of the method used to achieve abstinence (forced or voluntary). In contrast, one study that used different cocaine self-administration training conditions during adolescence reported data implicating BLA projections to nucleus accumbens in 'incubated' cocaine seeking after prolonged (45 d) forced abstinence (Lee et al., 2013).

Our pharmacological results agree with previous findings showing a role of CeA in reinstatement of cocaine seeking after extinction of the drug-reinforced responding (Alleweireldt et al., 2006; Kruzich and See, 2001). In these studies, CeA injections of either tetrodotoxin (a sodium channel blocker) or the Drd1 antagonist SCH23390 decreased reinstatement of cocaine seeking. However, unlike our negative data for BLA, in the above studies and other studies (Berglind et al., 2006; McLaughlin and See, 2003; See et al., 2001), BLA reversible inactivation or local dopamine receptor blockade decreased reinstatement of cocaine seeking after extinction.

What might account for the selective role of CeA but not BLA in relapse after prolonged abstinence (forced or voluntary) versus the role of both CeA and BLA in reinstatement after extinction? A likely reason is that the mechanisms of reinstatement after extinction are different from underlying relapse to drug seeking after abstinence (Fuchs et al., 2006; Marchant et al., 2013). For example, reversible inactivation of dorsal but not ventral mPFC decreases reinstatement of cocaine seeking after extinction (McLaughlin and See, 2003), while reversible inactivation of ventral but not dorsal mPFC decreases relapse to cocaine seeking after forced abstinence (Koya et al., 2009b). Additionally, reversible inactivation of either ventral or dorsal mPFC decreases reinstatement of methamphetamine seeking after extinction (Rocha and Kalivas, 2010), while inactivation of these regions has no effect on relapse to methamphetamine seeking after forced abstinence (Li et al., 2015b).

Role of anterior insular cortex and its projection to central amygdala

We found that relapse to methamphetamine seeking after voluntary abstinence was associated with selective activation of the AIV→CeA projection. Additionally, reversible inactivation of the AIV or the AIV→CeA projection decreased relapse after voluntary abstinence and relapse-associated CeA activation. Our data on the role of AIV in relapse after voluntary abstinence agrees with previous studies on the role of the anterior insular cortex in relapse to drug seeking in rat models. Thus, reversible inactivation of this brain region decreases cue-induced reinstatement of cocaine and nicotine seeking (Cosme et al., 2015; Pushparaj et al., 2015), and context-induced reinstatement of cocaine seeking (Arguello et al., 2017). Additionally, post-training lesions of the anterior insula decreased cocaine priming-induced reinstatement of cocaine seeking (Rotge et al., 2017).

We used electron microscopy to demonstrate that identified mCherry AIV neurons express vGluT1, which accumulates in terminal synaptic vesicles and form asymmetric synapses in CeA, with preferential innervation of CeL (Fig. 6). Asymmetric synapses are excitatory and typically glutamatergic (Zhang et al., 2015). Therefore, our data indicate that glutamate from the AIV projection is released via vGluT1 vesicles preferentially into CeL and plays a critical role in relapse after voluntary abstinence. In agreement with our electron microscopy findings, blocking action potential-induced activity within the CeA does not affect excitatory postsynaptic currents evoked by light stimulation of ChR2-expressing AIV terminals. Based on our pharmacological and RNAscope data on the role of CeA Drd1 in relapse after voluntary abstinence, a question for future research is whether AIV neurons activated during the relapse tests preferentially activate Drd1-expressing neurons in CeL.

The psychological mechanisms and downstream CeA targets that control relapse after voluntary abstinence are currently unknown. One possibility is that drug seeking during the relapse tests is due to an appetitive motivational state induced by exposure to drug-associated cues (Stewart et al., 1984). In this regard, CeA projections to lateral hypothalamus (Pitkanen, 2000), a critical brain region for relapse to drug seeking (Khoo et al., 2017; Marchant et al., 2014) and appetitive motivated behavior (Harris et al., 2005; Wise, 1996), could be a potential downstream target. Another possibility is that drug seeking during the relapse is due to a negative motivational state caused by the removal of the preferred alternative palatable food reward. This putative "frustrative non-reward" responding (Amsel, 1958), which may reflect stress-induced behavioral activation (Micioni Di Bonaventura et al., 2014), can recruit stress-associated downstream CeA projections, including the periaqueductal gray and bed nucleus of stria terminalis (BNST) (Gungor and Pare, 2016; Janak and Tye, 2015; Penzo et al., 2014; Sakanaka et al., 1986). In this regard, there is evidence that the CeA→BNST projection is critical to stress-induced reinstatement of cocaine seeking (Erb et al., 2001; Mantsch et al., 2016).

Finally, our results on the role of AIV in relapse after voluntary abstinence agree with previous clinical studies on insula's role in human drug addiction. Thus, in cocaine and methamphetamine addicts, exposure to drug-associated cues increase BOLD fMRI signal in the insula (Garavan et al., 2000; Yin et al., 2012), and in nicotine addicts, insula damage decreases relapse rates (Gaznick et al., 2014; Naqvi et al., 2007).

Methodological considerations

One methodological issue is that the effect of systemic or CeA SCH39166 injections on relapse is due to nonspecific performance deficits. This is unlikely because we used systemic or intracranial doses that had no effect on high-rate food-reinforced responding (Fig. S1). Another issue is that the effect of CeA SCH39166 injections is due to diffusion to nearby amygdala sub-nuclei. However, our data indicate that diffusion to the nearby BLA is unlikely to account for our results, because BLA SCH39166 injections were ineffective. Similarly, it is unlikely that the effect of AIV muscimol+baclofen injections on relapse is due to diffusion to the nearby OFC, because OFC injections were ineffective. However, we cannot rule out that dorsal diffusion of muchimol+baclofen to AID contributed to the effect of AIV inactivation on relapse.

Additionally, an issue to consider is that it was recently reported that CNO administration in absence of hM4Di or hM3Dq viral expression has behavioral effects in rats (MacLaren et al., 2016). Although these data were obtained with systemic CNO injections, we wanted to rule out the possibility that our selective inhibition of the AIV→CeA pathway was due to non-selective effects of CNO. We found that CNO injections into the CeA of virus-free rats had no effect on either relapse or relapse-test-induced local Fos expression. Additionally, bath application of CNO onto CeA neurons adjacent to hM4Di receptor-expressing AIV terminals (mCherry+), but not non-expressing terminals (mCherry-), decreased the amplitude of evoked synaptic response and frequency of spontaneous synaptic events. These results indicate that the behavioral effects of CNO on relapse are due to selective inhibition of the AIV→CeA pathway.

Finally, we found that only a small proportion (>10%) of Fos positive neurons in AIV were co-labeled with CTb (Fig. 3F). The projection targets and role of the CTb-negative/Fos-positive AIV neurons in relapse after voluntary abstinence is currently unknown. We speculate that these relapse-activated neurons project to other brain regions (e.g., nucleus accumbens, prefrontal cortex (Seif et al., 2013; Shi and Cassell, 1998; Wright and Groenewegen, 1996) that potentially contribute to drug seeking after voluntary abstinence. In this regard, we found that inhibition of CeA, AIV, and the AIV→CeA projections decreased active lever presses by ~40–60% but did not completely block drug seeking (i.e., similar active versus inactive lever responding during the relapse test), further supporting the notion that other brain areas and circuits contribute to relapse after voluntary abstinence. Indeed, as mentioned in the Introduction, we recently identified a role of dorsomedial striatum neuronal ensembles in this form of relapse (Caprioli et al., 2017).

Conclusions

We recently developed a choice-based rat model of drug relapse and craving after voluntary abstinence (Caprioli et al., 2015a) and proposed that our model mimics features of human relapse after cessation of voucher-based contingency management (Higgins et al., 2004; Roll, 2007). Here, we used pharmacological, anatomical, physiological, and chemogenetic approaches to show a critical role of Drd1-mediated CeA neuronal activity and monosynaptic AIV→CeA glutamatergic projection that preferentially innervate the CeL in relapse after cessation of contingency management in a rat model. Finally, to the degree that results from rat relapse models can be generalized to humans (Epstein et al., 2006) and to the degree that choice of palatable food over a drug in the rat mimics choice of monetary voucher of a drug in humans, our first circuit characterization of relapse to drug seeking after voluntary abstinence suggests the insular cortex projections to central amygdala as a potential novel target for relapse prevention, using different brain stimulation/inhibition methods like deep-brain transcranial magnetic stimulation (TMS) (Feil and Zangen, 2010).

Star methods

Contact for reagent and resource sharing

Materials, datasets, and protocols are available upon request to the corresponding author, Yavin Shaham (Yshaham@intra.nida.nih.gov)

Experimental model and subject details

We used male Sprague-Dawley rats (Charles River, total n=249), weighing 300–350 g. We housed the rats two per cage for 1–3 weeks, and then housed them individually after surgery. We maintained the rats on a reverse 12-h light/dark cycle (lights off at 8 AM) with free access to standard laboratory chow and water. Our procedures followed the guidelines outlined in the Guide for the Care and Use of Laboratory Animals (8th edition; http://grants.nih.gov/grants/olaw/Guide-for-the-Care-and-Use-of-Laboratory-Animals.pdf). We excluded 32 rats, due to sickness (n=6), misplaced cannula placements (n=15), or low CTb (n=4) or viral expression (n=5, Exp. 5 and n=2, Exp.6).

Methods details

Surgery—We performed all surgeries except the CTb injections (see below and Exp. 3) before palatable food and methamphetamine self-administration training. We anesthetized the rats with isoflurane (5% induction; 2–3% maintenance) and injected ketoprofen (2.5 mg/kg, s.c. Butler Schein) after surgery and the following day to relieve pain and decrease inflammation; we allowed the rats to recover from surgery for 6–7 days before food self-administration training.

Intravenous surgery: We inserted silastic catheters into the jugular vein as described previously (Caprioli et al., 2015a). We placed the distal end of the catheters into the jugular vein and attached the proximal end to a modified 22-gauge cannula to be placed on the back in the mid scapular region. We flushed the catheters daily with 0.2 ml of sterile saline solution containing 0.85 mg of gentamicin (APP Pharmaceuticals; 4.25 mg/mL).

Intracranial surgery: We implanted guide cannulas (23 gauge; Plastics One) 1 mm above the target sites. We set the nose bar at −3.3 mm and used the following coordinates from Bregma: CeA: anterior-posterior (AP), −2.5 mm; medial-lateral (ML), ±4.5 mm (2° angle); dorsal -ventral (DV), −7.5 mm. BLA: AP, −2.5 mm; ML, ±5.3 mm (2° angle); DV, −7.8 mm. AIV: AP, +2.8; ML, ±4.9 (10° angle); DV, −5.2 mm. OFC: AP, +3.1 mm; ML, ±3.5 mm (10° angle); DV, −5.0 mm. We anchored the cannulas to the skull with jeweler's screws and dental cement. We used the above coordinates based on pilot and previous studies (Li et al., 2015b; Lu et al., 2005a; Pelloux et al., 2013).

CTb injection into CeA: We performed the CTb injections between the self-administration training and voluntary abstinence phases. We unilaterally injected 20 nl of 1% CTb (List Biological Laboratories) into CeA over 5 min with the needle left in place for an additional 5 min (Marchant et al., 2016; Marchant et al., 2009; Marchant et al., 2014). We injected CTb into either the left or right hemisphere (counterbalanced) using a 1.0 µl, 32-gauge "Neuros" syringe (Hamilton) attached to UltraMicroPump (UMP3) with SYS-Micro4 Controller (World Precision Instruments). CeA coordinates: AP, −2.5; ML, ±4.5 (10° angle); DV, −8.5 mm from Bregma.

Viral injections: We bilaterally injected AAV8-hSynp-hM4Di-mCherry [Exp. 5 and Exp.6] (UNC vector core) into AIV: AP, +2.8; ML, ±4.9 (10°angle); DV, −6.2 mm from Bregma. We injected 0.75 µl over 5 min and left the needle in place for 5 min. We used 10 µl Nanofil

syringes (World Precision Instruments) with 33-gauge needles, attached to an UltraMicroPump (UMP3) with SYS-Micro4 Controller (World Precision Instruments).

Drugs—We received (+)-methamphetamine-HCl (methamphetamine) from NIDA pharmacy and dissolved it in sterile saline. We chose a unit dose of 0.1 mg/kg for self-administration training based on our previous studies (Caprioli et al., 2015a; Krasnova et al., 2014; Li et al., 2015b). In Exp.1 we dissolved SCH39166 (Tocris Bioscience) in ethanol (1 μg/μl) and then diluted it with sterile saline for a final concentration of 20 μg/ml. We injected vehicle (1 ml/kg) or SCH39166 (20 μg/kg, s.c) 30 min before the start of the test sessions. The dose of SCH39166 is based on previous studies (Caine and Koob, 1994; Ciccocioppo et al., 2001; Weiss et al., 2001) and on a pilot study in which we found that at doses of 5, 10 and 20 μg/kg, SCH39166 had no effect on operant responding for food pellets (Fig. S1A). In Exp. 2 we dissolved SCH39166 and raclopride (Sigma Aldrich) in sterile saline (2 mg/ml) and injected the drugs bilaterally into CeA (SCH39166 and raclopride) and BLA (SCH39166) at doses of 0.5 and 1.0 μg/0.5 μl/side (15 min pretreatment time). These doses are based on previous studies in which raclopride was injected into the amygdala (Berglind et al., 2006) and our studies using a related Drd1 antagonist, SCH23990 (Bossert et al., 2012; Bossert et al., 2009). In Exp. 4, we dissolved muscimol + baclofen (M+B) (Tocris Bioscience) in sterile saline and injected it bilaterally into AIV or OFC at a dose of (50+50) ng/0.5 μl/side (15 min pretreatment time). The doses of muscimol and baclofen are based on previous studies (McFarland and Kalivas, 2001; Stopper and Floresco, 2014). In Exp. 5 we dissolved CNO (Tocris Bioscience) in sterile saline and injected bilaterally into the CeA at a dose of 1.0 mM/0.5 μl/side (15 min pretreatment time). This dose is based on a previous study in which CNO selectively inhibited ventral pallidum terminals in ventral tegmental area during a reinstatement to cocaine seeking test (Mahler et al., 2014).

Intracranial injections—We connected the syringe pump (Harvard Apparatus) to 10-μl Hamilton syringes and attached the Hamilton syringes to 30-gauge injectors via polyethylene-50 tubing; the injectors extended 1 mm below the tips of the guide cannulas. We made all intracranial injections over 1 min and left the injectors in place for an additional minute to allow diffusion. After the final tests, we anesthetized the rats, removed their brains, and stored the brains in 10% formalin. Using a cryostat (Leica Microsystems), we sectioned the brains (40 μm), stained them with Cresyl Violet, and verified cannula placements under a light microscope. In Exp. 5 after the final tests, we perfused the rats for subsequent immunohistochemistry (see below).

Immunohistochemistry—Immediately following the behavioral tests, we anesthetized the rats with isoflurane and perfused them transcardially with ~100 mL of 0.1 M phosphate-buffered saline (pH 7.4) (PBS) followed by ~400 mL of 4% paraformaldehyde (PFA) in PBS. We removed the brains and post-fixed them in 4% PFA for 2 h before transferring them to 30% sucrose in PBS for 48-h at 4°C. We froze the brains in dry ice and stored the m at −80°C. We cut coronal sections (40 μm) of the different brain areas using a Leica cryostat. We collected the tissue in cryoprotectant (20% glycerol and 2% DMSO in 0.1 M PBS, pH 7.4) and stored them at −80 °C until further processing (Exp. 1 and 5) or collected sections in PBS containing 0.1% sodium azide and stored them at 4 °C (Exp. 3).

Fos labeling (Exp. 1): We rinsed free-floating sections (3 × 10 min) in PBS, incubated them for 1 h in 3% normal goat serum (NGS) in PBS with 0.25% Triton X-100 (PBS-Tx), and incubated them overnight at 4 °C with rabbit anti-c-Fos primary antibody (Phospho-c-Fos, 5348S, Cell Signaling Technology; RRID: AB_10557109) diluted 1:8000 in 3% NGS in PBS-Tx. We then rinsed the sections in PBS and incubated them for 2 h with biotinylated anti-rabbit IgG secondary antibody (BA-1000, Vector Laboratories) diluted 1:600 in 1% NGS in 0.25% PBS-Tx. We rinsed the sections again in PBS and incubated them in avidin–biotin–peroxidase complex (ABC; ABC Elite kit, PK-6100, Vector Laboratories) in 0.5% PBS-Tx for 1 h. We then rinsed the sections in PBS, developed them in 3,3′-diaminobenzidine (DAB) in 0.3% hydrogen peroxide (H_2O_2), rinsed them in PBS for 30 min, mounted them onto chrome alum/gelatin-coated slides, and air-dried them. We dehydrated the slides through a graded series of alcohol concentrations (30, 60, 90, 95, 100, 100 % ethanol), cleared the slideswith Citrasolv (Fisher Scientific), and cover slipped them with Permount (Fisher Scientific).

CTb injection site verification (Exp. 3): The immunohistochemical procedure was based on our previously published work (Marchant et al., 2016; Marchant et al., 2014). We selected a 1-in-4 series of 40 μm sections from CeA of each rat and used immunofluorescence to determine CTb injection sites. We repeatedly rinsed free-floating sections in PBS (3 × 10 min) and incubated them for 2 h in 0.5% PBS-Tx with 10% normal horse serum (NHS). We then incubated all sections for at least 48 h at 4 °C in goat anti-CTb primary antibody (1:50 00, List Biological Laboratories, 703; RRID: AB_10013220) diluted in 0.5 % PBS-Tx with 2% NHS. We rinsed off unbound primary antibodies with PBS and incubated the sections for 4 h in 0.5 % PBS-Tx with 2% NHS and donkey anti-goat Alexa Fluor 488 (1:2000; Jackson ImmunoResearch, 705-546-147; RRID: AB_2340430). We then rinsed the sections in PBS, mounted onto gelatin-coated glass slides, air-dried, and cover-slipped with mowiol (Millipore).

Fos and CTb double-labeling (Exp. 3): We processed a 1-in-4 series of AI, vmPFC, PVT, BLA, and vSub for immunohistochemical detection of Fos-protein and CTb. We rinsed free-floating sections (3×10 min) and then incubated them in 10% NHS with 0.5 % PBS-Tx for 2 h. We then incubated the sections for at least 48 h at 4 °C in 0.5 % PBS-Tx containing 2% NHS and rabbit anti-c-Fos primary antibody (1:8000, Cell Signaling Technology, Phospho-c-Fos, 5348S; RRID: AB_10013220) and goat anti-CTb primary antibody (1:5000, CTb 703; List Biological Laboratories; RRID: AB_10013220). We rinsed the sections in PBS and incubated them for 3 h in PBS containing 2% NHS and donkey anti-rabbit Alexa Fluor 594 (711-585-152; RRID: AB_2340621; Jackson ImmunoResearch) and donkey anti-goat Alexa Fluor 488 (705-546-147; RRID: AB_2340430; Jackson ImmunoResearch) diluted to 1:2000. We rinsed the sections in PBS (3 × 10 min) and mounted them onto gelatin-coated slides, partially dried, and coverslipped the sections with Vectashield Hard Set Mounting Medium (H-1400; Vector Laboratories).

NeuN and mCherry double-labeling (Exp. 5): We selected a 1-in-4 series of sections from AIV of each rat, and used immunofluorescence to determine the percentage of DREADD (mCherry-positive) neurons co-labeled with NeuN (a neuronal marker). We also sectioned

CeA to check cannula placements and AIV terminal projection expression. We excluded rats with mCherry/NeuN percentage expression lower than 15% (n=5). We rinsed free-floating sections in PBS (3×10 min), incubated for 1 h in 4% bovine serum albumin (BSA) in 0.3% PBS-Tx, and incubated the sections overnight at 4 °C with mouse anti-mCherry primary antibody (Clontech Laboratories, 632543; RRID: AB_2307319) diluted 1:500 in 4% BSA in 0.3% PBS-Tx. We rinsed the sections in PBS and incubated them for 2 h with biotinylated anti-mouse IgG secondary antibody (Vector Labs, BA-9200; RRID: AB_2336171) diluted 1:600 in 4% BSA in 0.3% PBS-Tx. We again rinsed the sections in PBS and incubated them in avidin-biotin-peroxidase complex (ABC; ABC Elite kit, PK-6100, Vector Laboratories) in 0.5% PBS-Tx for 1 h. We rinsed the sections in PBS and developed them in Vector SG (blue/gray product; Vector SG peroxidase substrate kit, Vector Laboratories). We stopped the reaction by rinsing the sections several times and incubating them for 1 h in 0.3% PBS-Tx containing 4% bovine serum albumin (BSA) and avidin D (avidin-biotin blocking kit; Vector Laboratories). We then incubated the sections overnight at 4 °C with mouse anti-NeuN primary ant ibody (MAB377, Millipore; RRID: AB_2298772) diluted 1:2000 in 4% BSA, 0.3% PBS-Tx, and biotin. We rinsed the sections in PBS and incubated them for 1 h with biotinylated anti-mouse IgG secondary antibody (Vector Labs, BA-9200; RRID: AB_2336171) diluted 1:500 in 4% BSA in 0.3% PBS-Tx. We rinsed the sections again in PBS and incubated them in ABC in PBS for 1 h. After rinsing the sections in PBS, we developed them in 3,3-diaminobenzidine (DAB), rinsed them in PBS, mounted them onto chrome alum/ gelatin-coated slides, and air-dried the sections. We dehydrated the slides through a graded series of alcohol concentrations (30, 60, 90, 95, 100, 100% ethanol), cleared with Citrasolv (Fisher Scientific), and coverslipped them with Permount (Fisher Scientific).

Fos labeling (Exp. 5): We processed a 1-in-4 series of CeA for immunohistochemical detection of Fos protein. We rinsed free-floating sections in PBS (3×10 min) and then incubated them in 10% NHS with 0.5 % PBS-Tx for 2 h. We then incubated the sections for at least 48 h at 4 °C in 0.5 % PBS-Tx containing 2% NHS and rabbit anti-c-Fos primary antibody (1:8000, Cell Signaling Technology, Phospho-c-Fos, 5348S; RRID: AB_10013220). We rinsed the sections in PBS and incubated them for 3 h in PBS containing 2% NHS and donkey anti-rabbit Alexa Fluor 594 (711-585-152; RRID: AB_2340621; Jackson ImmunoResearch) diluted to 1:2000. We rinsed the sections three times in PBS (3×10 min) and mounted them onto gelatin-coated glass slides, air-dried, and cover-slipped the sections with mowiol + DAPI (Millipore).

RNAscope® *in situ* hybridization assay (Exp. 1)—We performed RNA *in situ* hybridization (ISH) for *Fos*, *Drd1*, and *Drd2* mRNAs as described previously (Caprioli et al., 2017; Li et al., 2015a; Rubio et al., 2015; Warren et al., 2016). Sixty min after the beginning of the test session, we briefly anesthetized the rats with isoflurane and decapitated them. We rapidly extracted and froze their brains for 20 s in –40°C isopentane. We store d brains at –80°C until use. We then collected CeA and BLA coronal sections (16 μm) directly onto Super Frost Plus slides (Fisher Scientific). We used RNAscope® Multiplex Fluorescent Reagent Kit (Advanced Cell Diagnostics) and performed ISH assay according to the user manual for fresh frozen tissue and as described previously (Caprioli et al., 2017; Li et al.,

2015a; Rubio et al., 2015; Warren et al., 2016). On the first day, we fixed the brain sections in 10% neutral buffered formalin (Fisher Scientific) for 20 min at 4°C. We rinsed the slides three times in PBS and dehydrated the slides in 50, 70, 100, and 100% ethanol. We stored the slides in fresh 100% ethanol overnight at −20°C. On the second day, we first dried the slides at room temperature for 10 min. To limit the spreading of the solutions, we drew a hydrophobic barrier on slides around brain sections.

We then treated the slides with protease solution (pretreatment 4) at room temperature for 20 min and then washed it off. We then applied target probes for *Fos*, *Drd1*, and *Drd2* to the slides and incubated them at 40°C for 2 h in a HybEZ oven. Each RNAscope® target probe contains a mixture of 20 ZZ oligonucleotide probes that are bound to the target RNA: *Fos*-C3 probe (GenBank accession number NM_022197.2; target nt region, 473–1497); *Drd1*-C1 probe (GenBank accession number NM_012546.2; target nt region, 104 – 1053), and *Drd2*-C2 probe (GenBank accession number NM_012547.1; target nt region, 445–1531). Next, we incubated the slides with preamplifier and amplifier probes (AMP1, 40°C for 3 0 min; AMP2, 40°C for 15 min; AMP3, 40°C for 30 min). We then incubated the slides with fluorescently labeled probes by selecting a specific combination of colors associated with each channel: green (Alexa 488 nm), orange (Alexa 550 nm), and far red (Alexa 647 nm). We used AMP4 Alt4 to detect triplex *Fos*, *Drd1*, and *Drd2* in far red, green, and red, respectively. Finally, we incubated the sections for 20 s with DAPI. After air-drying the slides, we cover-slipped them with a Vectashield fluorescent mounting medium (H-1400; Vector Laboratories).

Self-administration apparatus—We trained rats to self-administer methamphetamine in chambers as described previously (Caprioli et al., 2015a; Caprioli et al., 2017; Caprioli et al., 2015b; Venniro et al., 2017). Briefly, we equipped each self-administration chamber with a stainless-steel grid floor and 2 operant panels. We equipped the left panel of the chamber with a discriminative stimulus (red light – Med Associates ENV-221M, red lens) that signaled the insertion and subsequent availability of the methamphetamine-paired active (retractable) lever. We equipped the right panel of the chamber with a discriminative stimulus (white house light - Med Associates ENV-215M) that signaled the insertion and subsequent availability of the food-paired active (retractable) lever. We equipped the right wall with an inactive (stationary) lever; presses on this lever had no reinforced consequences. We placed a bottle of water and a food hopper on the external and internal side of the chamber's transparent polycarbonate door, respectively.

<u>**Food pellet self-administration:**</u> Our training procedure is like that described elsewhere (Caprioli et al., 2015a; Caprioli et al., 2017; Caprioli et al., 2015b; Venniro et al., 2017). We trained the rats to lever press for food during two1-h daily sessions that were separated by 10 min under a fixed-ratio-1 (FR1), 20-s timeout reinforcement schedule, which led to the delivery of five 45-mg 'preferred' or palatable food pellets (TestDiet, Catalogue # 1811155, 12.7% fat, 66.7% carbohydrate, and 20.6% protein) (Calu et al., 2014); pellet deliveries were paired with the 20-s discrete tone cue (Med Associates ENV-223AM) and the 5 pellets were delivered 1 s apart. Prior to the first 1–2 formal operant training sessions, we gave the rats 1-h magazine training sessions during which 5 pellets were delivered non-contingently every 5

min. The sessions began with the presentation of the white house light followed 10 s later by the insertion of the food-paired active lever; the white houselight remained on for the duration of the session and served as a discriminative stimulus for the palatable food. At the end of the session, the white light was turned off and the active lever was retracted. We used this 'preferred' TestDiet pellet type in our previous studies (Calu et al., 2014; Caprioli et al., 2015a; Caprioli et al., 2015b; Cifani et al., 2012; Pickens et al., 2012). To match the number of discrete cue presentations to that of methamphetamine (see below), we limited the number of food reward deliveries to 15 per h.

Methamphetamine self-administration: We trained rats to self-administer methamphetamine during two 1-h daily sessions that were separated by 10 min under an FR1 20-s timeout reinforcement schedule; drug infusions were paired with the 20-s discrete white light cue (Med Associates ENV-221M, white lens). The sessions began with the presentation of the red light for 10 s followed by the insertion of the methamphetamine-paired active lever; the red light remained on for the duration of the session and served as a discriminative stimulus for methamphetamine availability. At the end of each 1-h session, the red light was turned off, and the active lever was retracted. The rats self-administered the drug at a dose of 0.1 mg/kg/infusion over 3.5 sec (0.1 ml/infusion). To prevent overdose, we limited the number of infusions to 15 per h.

Discrete-trials choice procedure: We conducted the discrete choice sessions using the same parameters (dose of methamphetamine, number of palatable food pellets per reward, stimuli associated with the two retractable levers) that we used during the training phase. We allowed the rats to choose between the methamphetamine- and the palatable food-paired lever in a discrete-trials choice procedure. We divided each 200 min choice sessions into 20 discrete trials that were separated by 10 min as previously described (Caprioli et al., 2015a; Caprioli et al., 2015b; Lenoir and Ahmed, 2008; Lenoir et al., 2007). Briefly, each trial began with the presentation of both discriminative stimuli previously associated with palatable food or methamphetamine followed 10 s later by the insertion of both the palatable food- and methamphetamine-paired levers. Rats then had to select one of the two levers. If the rats responded within 8 min, they only received the reward corresponding with the selected lever. Thus, on a given trial, the rat can either earn the drug or the food reward, but not both. Each reward delivery was signaled by the methamphetamine- or food-associated cue (white cue light or tone, respectively), the retraction of both levers, and the shut-down of the food- and methamphetamine discriminative cues. If a rat failed to respond on either active lever within 8 min, both levers were retracted and their related discriminative cues were shut-down with no reward delivery (Caprioli et al., 2015a; Caprioli et al., 2015b). We introduced two choice sessions during the training phase to assess whether the choice behavior changes over time during this phase.

Voluntary abstinence: After completion of the training phase, we allowed the rats to choose between the methamphetamine-paired lever (delivering 1 infusion) and palatable food-paired lever (delivering 5 pellets) during 20 discrete-choice trials for 14 daily sessions, as described above.

Relapse test: The relapse test in the presence of the methamphetamine-associated cues consisted of a single 60 to 120 min session (see specific experiments) on voluntary abstinence day 15. The sessions began with the presentation of the red discriminative cue light, followed 10 s later by the insertion of the methamphetamine-paired active lever; the red light remained on for the duration of the session. Active lever presses during testing, the operational measure of drug seeking in forced abstinence and incubation of craving studies (Lu et al., 2004; Pickens et al., 2011; Venniro et al., 2016), resulted in contingent presentations of the light cue, previously paired with drug infusions, but not methamphetamine (Caprioli et al., 2015a; Krasnova et al., 2014; Li et al., 2015b; Theberge et al., 2013). Based on our previous studies (Bossert et al., 2011; Caprioli et al., 2017; Li et al., 2015b) and the time course of Fos induction (Morgan and Curran, 1991), the relapse tests were 60 or 90 min in experiments in which we measured Fos mRNA or protein expression, respectively. In experiments in which we only tested the effect of dopamine receptor antagonists on relapse, the test duration was 2 h (the duration of the training session).

Specific experiments

Exp. 1: Effect of systemic injections of Drd1 antagonist on relapse to methamphetamine seeking, Fos expression and cell type specificity in CeA and BLA:

We used 4 groups of rats (n=8–14 per group) in an experimental design that included the between-subjects factors of SCH39166 dose (0, 20 μg/kg, s.c.; 30 min pretreatment time) and Test condition (No test, Relapse test). For the RNAscope® *in situ* hybridization, we used two groups of rats (n=5–6 per group) in an experimental design that included the between-subjects factors of Test condition (No test, Relapse test).

This experiment and Exp. 2–5 described below consisted of 3 phases: self-administration training (3 weeks), voluntary abstinence (14 days), and relapse tests that were performed one day after the last voluntary abstinence day. We matched the rats in the different groups of Exp. 1 (and in all the other experiments) for methamphetamine intake during the training phase. On test days, we brought the rats from the No-test groups directly from their home cage and perfused them at the same time with the rats from the Relapse test groups.

Exp. 2: Effect of Drd1 or Drd2 antagonist injections into the amygdala on relapse to methamphetamine seeking after voluntary abstinence:

We first tested 3 groups of rats (n=8 per group) for the effect of CeA vehicle or SCH39166 (0.5 or 1.0 μg/side; 15 min pretreatment time) injections on non-reinforced lever presses during the relapse tests (2 h). We next tested 2 groups of rats (n=9 per group) for the effect of BLA vehicle or SCH39166 (1.0 μg/side) on relapse (a test for anatomical specificity). Finally, we tested 3 groups of rats (n=6–7 per group) for the effect of CeA vehicle or raclopride (0.5 or 1.0 μg/side, 15 min pretreatment time) on relapse (a test for pharmacological specificity). At the end of the experiment, we retrained some of the rats with CeA cannulas (n=22) to lever press for food for 3 days. We then tested them for the effect of SCH39166 (0.5 or 1.0 μg/side) on lever pressing for food to verify that the drug's effect on relapse to is not due to non-selective effects on operant responding (Fig. S1B).

Exp. 3: Effect of relapse to methamphetamine seeking after voluntary abstinence on Fos expression in afferent projections to CeA: We injected CTb into the CeA one day after the last self-administration session and started the voluntary abstinence phase 4 days after these injections. We used two groups of rats (n=4 per group) in an experimental design that included the between-subjects factors of Test condition (No test, Relapse test). On the test day, we brought the rats from the No-test group directly from their home cage and perfused them at the same time with the rats from the Relapse test group.

Exp. 4: Effect of GABA$_A$ + GABA$_B$ receptor agonist injections in the AIV on relapse to methamphetamine seeking after voluntary abstinence: We first tested 2 groups of rats (n=10–12 per group) for the effect of AIV vehicle or M+B (50 ng+50 ng/0.5 μL/side, 15 min pretreatment time) on relapse. We then tested 2 separate groups of rats (n=8 per group) for the effect of OFC vehicle or M+B (50 ng+50 ng/side) on relapse to methamphetamine seeking (a test for anatomical specificity). At the end of the experiment, we retrained some of the rats with AIV cannulas (n=8) to lever press for food for 3 days. We then tested them for the effect of vehicle or M+B over 3 days on lever pressing for food to verify that the drug's effect on relapse to methamphetamine seeking is not due to non-selective effects on operant responding (Fig. S1C).

Exp. 5: Effect of CNO injections in the CeA on relapse to methamphetamine seeking after voluntary abstinence: We tested 2 groups of rats (n=15 per group) for the effect of CeA vehicle or CNO (1.0 mM/side, 5 min pretreatment time) on relapse to drug seeking. We next used 2 groups of rats (n=8–9 per group) to determine whether CeA injections of CNO without the hM4Di virus injection would affect relapse to after voluntary abstinence. We determined the effect of CNO alone (without DREADD virus) on relapse, because of a recent study showing that CNO can induce hM4Di- or hM3Di-independent effects in rats (MacLaren et al., 2016). In addition, we measured Fos expression in all groups of rats to determine whether CNO injections in hM4Di-injected rats decrease CeA neuronal activity.

Exp. 6: electron microscopy characterization of the AIV→CeA projection: The goal of this final experiment was to anatomically characterize the AIV→CeA projection and to ascertain that AIV neurons projecting to CeA form asymmetric (presumably excitatory) synapse on CeA cell bodies.

Tissue Preparation: We injected AAV8-hSynp-hM4Di-mCherry into AIV of rats (n=5). After six weeks, we anesthetized 5 rats with chloral hydrate (35 mg/100 g) and perfused them transcardially with a 4% PFA, 0.15% glutaraldehyde, and 15% picric acid solution in 0.1M PB, pH 7.3. We kept brains in this solution for 2 h at 4 °C and then we transferred to a 2% PFA solution at 4 °C overnight. For sectioning, we rinsed the brains with PB and then cut a serial 50-μm thick coronal sections, using a vibratome (VT1000S, Leica, Vienna, Austria). We excluded 2 rats because of misplaced viral expression.

Confocal microscopy: We incubated free-floating coronal sections (50 μm) (n=3) in PB supplemented with 4% BSA and 0.3% Triton X-100 for 1 h. We then incubated the sections with cocktails of primary antibodies (mouse anti-mCherry [1:500, Clontech Laboratories, 632543; RRID: AB_2307319] + guinea pig anti-vGluT1 [1:500, Frontier Institute, vGluT1-

GP-Af570; RRID: AB_2571534]) overnight at 4°C. After rinsing 3×10 min in PB, we incubated the sections in a cocktail of the corresponding fluorescence secondary antibodies (Alexa Fluor 488– anti–guinea pig [706-545-148 RRID: AB_2340472] + Alexa Fluor 594– anti-mouse [715-586-151 RRID: AB_2340858] Jackson Immunoresearch Laboratories, 1:100 dilution) for 2 h at room temperature. After rinsing, we mounted sections on slides. We collected fluorescent images with an Olympus FV1000 Confocal System (Olympus). We took images sequentially with different lasers with 10X or 100X oil immersion objectives and we collected z-axis stacks at 0.2 µm. We successfully repeated this procedure three times.

Immuno-electron microscopy: As previously described (Zhang et al., 2015), we rinsed and incubated the vibratome-cut sections in 1% sodium borohydride to inactivate free aldehyde groups, rinsed, and then incubated with a blocking solution. We then incubated the sections with primary antibodies (mouse anti-mCherry (1:500; Clontech Laboratories, 632543; RRID: AB_2307319) and guinea pig anti-vGluT1 (1:500; Frontier Institute, vGluT1-GP-Af570; RRID: AB_2571534)). We diluted all primary antibodies in PB with 1% NGS, 4% BSA in PB supplemented with 0.02% saponin. We incubated sections for 24 h at 4°C. We rinsed and again incubated sections overnight at 4 °C in the corresponding secondary antibodies. We then rinsed the sections in PB, and then in double-distilled water, followed by silver enhancement of the gold particles with the Nanoprobes Silver Kit (2012, Nanoprobes) for 7 min at room temperature. Next, we incubated the sections in avidin-biotinylated horseradish peroxidase complex in PB for 2 h at room temperature and then washed them. We detected peroxidase activity with 0.025% 3,3'-diaminobenzidine (DAB) and 0.003% H_2O_2 in PB for 5–10 min. We then rinsed sections with PB and fixed them with 0.5% osmium tetroxide in PB for 25 min; next, we washed the sections in PB followed by double-distilled water and then contrasted them in freshly prepared 1% uranyl acetate for 35 min. We dehydrated the sections through a series of graded alcohols and propylene oxide. Afterward, we flat embedded the sections in Durcupan ACM epoxy resin (14040, Electron Microscopy Sciences). We then polymerized resin-embedded the sections at 60°C for 2 d. We cut 65 nm of the sections from the outer surface of the tissue with an ultramicrotome UC7 (Leica Microsystems) using a diamond knife (Diatome). We collected the sections on formvar-coated single slot grids and counterstained them with Reynolds lead citrate. We examined and photographed sections using a Tecnai G2 12 transmission electron microscope (Fei Company) equipped with a digital micrograph OneView camera (Gatan).

Ultrastructural analysis of brain tissue: We collected serial ultra-thin sections of CeA from 3 rats. We classified synaptic contacts per their morphology and then we immunolabeled and photographed them at a magnification of 6,800–13,000X. We used the morphological criteria for identification and classification of cellular components or type of synapse observed in these thin sections as previously described by Zhang et al. (2015). In the serial sections, we considered a terminal an immunopositive terminal if it contained more than five immunogold particles. We adjusted the pictures to match contrast and brightness using Adobe Photoshop (Adobe Systems Incorporated). We successfully repeated this procedure three times. We performed the electron microscopy and confocal analysis in a blind manner.

Quantification and statistical analysis

Image acquisition and neuronal quantification—For cannula placements (Fig. S3) and immunohistochemistry image acquisition, we used an EXi Aqua camera (QImaging) attached to a Zeiss Axio Scope Imager M2 using iVision (4.0.15 and 4.5.0, Biovision Technologies). For the RNAscope® *in situ* hybridization image acquisition, we used an Olympus VS 120 microscope and ImageJ software for quantification.

Fos quantification (Exp. 1): We captured bright field images for Fos immunoreactive (IR) cells in CeA and BLA using a 5X objective. We also quantified Fos expression in CeL and CeM sub-regions of CeA. We analyzed the sections of the amygdala subregions within the Bregma coordinates of −1.8 to −3.3 mm. For each rat, we identified Fos-IR cells by a brown reaction product in the nuclei. We quantified cells in two hemispheres of 4 sections and computed the mean of these counts per area. We performed the image-based quantification in a blind manner (inter-rater reliability for CeA/BLA counting between M.V. and C.C. r=0.95, p<0.05, and for CeL/CeM between M.V. and M.Z. r=0.94, p<0.05).

Fos and CTb quantification (Exp. 3): We captured each image using a 10X objective. Each image comprised of 5 images through the z plane that we digitally collapsed using iVision, giving a single plane view of in-focus cells. For each rat, we quantified cells in the same hemisphere as the CTb injection in the following Bregma coordinates: vmPFC (+3.72 to +.2.76), AIV and dorsal anterior insular cortex (AID) (+3.72 to +0.48 mm); CeA BLA, and PVT (-1.8 to −3.3 mm); and vSub (-5.00 to −6.2). We performed the image-based quantification of CTb-IR, Fos-IR, and CTb+Fos-IR cells in a blind manner (inter-rater reliability between M.V. and C.C. r=0.93, p<0.05).

NeuN and mCherry quantification (Exp. 5): We captured bright field images for mCherry- and NeuN-IR cells in AIV using a 20X objective. We identified NeuN-IR cells by a brown product in the cytoplasm, mCherry-IR cells by a dark blue reaction product in the nuclei, and double-labeled cells by a dark blue nucleus surrounded by brown cytoplasm. For each rat, we quantified cells in two hemispheres of 4 sections and we averaged the counts to give a mean number of each immunoreactive cell type. We performed the image-based quantification in a blind manner (inter-rater reliability between M.V. and M.Z. r=0.93, p<0.05).

Fos quantification (Exp. 5): We captured each image using a 10X objective. For each rat, we quantified CeA-Fos positive cells in the area immediately underneath the cannula placement. We performed the image-based quantification cells in a blind manner (inter-rater reliability between M.V. and M.Z. r=0.96, p<0.05).

RNAscope® *in situ* hybridization quantification (Exp. 1): We captured each image using a 20X objective. We quantified the total number of *Drd1* (green) and *Drd2* (red) positive cells for each brain area (CeA, BLA, as well as Ce and CeM). We quantified the total *Fos* positive cells (white dots surrounding DAPI positive cells in blue). We also quantified the *Fos*-positive neurons co-labeled with *Drd1* or *Drd2*. We performed the image-based quantification in a blind manner (mean inter-rater reliability for CeA/BLA between M.V.

and D.C.: r=0.89, p<0.05; M.V. and M.Z.: r=0.92, p<0.05; D.C. and B.L.W. r=0.91, p<0.05; for CeL/CeM between M.V. and M.Z. r=0.90, p<0.05).

Glutamatergic terminal quantification in CeL and CeM (Exp. 6): We collected fluorescent images with an Olympus FV1000 Confocal System (Olympus). We took images sequentially with different lasers with 10X or 100X oil immersion objectives and Z-axis stacks were collected at 0.5 μm. We used Imaris microscopy software (Bitplane) to analyze Z-axis stacks of confocal images from 3 injected rats ($126 \times 126 \times 2$ μm for each image, 4 images of CeL and 4 images of CeM from each rat) to obtain 3-D quantification of axon terminals expressing mCherry or vGluT1. We repeated this procedure three times. We performed the image-based quantification in a blind manner (mean inter-rater reliability between M.V. and M.Z.: r=0.90, p<0.05).

Ex vivo electrophysiology

***Ex vivo* brain slice electrophysiology:** We performed *ex vivo* electrophysiology 4–8 weeks after intracranial viral delivery surgery into the AIV (n=6 for DREADD experiment, n=5 for TTX experiment). On the recording days, we deeply anesthetized the rats with isoflurane (90–120 s) and then transcardially perfused them with ice-cold solution containing the following (in mM): 92 NMDG, 20 HEPES, 25 Glucose, 30 $NaHCO_3$, 1.2 NaH_2PO_4, 2.5 KCl, 5 Na-ascorbate, 3 Na-pyruvate, 2 Thiourea, 10 $MgSO_4$, 0.5 $CaCl_2$, saturated with 95% O_2 5% CO_2 (pH 7.3–7.4, ~305 mOsm/kg). We cut coronal sections containing CeA in the ice-cold solution and incubated the slices for 10 min at 35°C in the same solution. We allowed the slices to recover for a minimum of 1 h at room temperature in ACSF containing the following (in mM): 126 NaCl, 2.5 KCl, 1.2 $MgCl_2$, 2.4 $CaCl_2$, 1.2 NaH_2PO_4, 21.4 $NaHCO_3$, 11.1 glucose, 3 Na-pyruvate, 1 Na-ascorbate. We recorded from the slices while they were bath-perfused (2.5 ml/min) at 32°C–35°C in the same ACSF solution with the addition of 50 μM picrotoxin to block $GABA_A$ receptors. For the TTX experiment, we added 10 μM 4-AP to the ACSF for the duration of the experiment to block potassium channels. The intracellular solution contained the following (in mM): 120 CsMeSO3, 5 NaCl, 10 TEA-Cl, 10 HEPES, 4 QX-314, 1.1 EGTA, 4 Mg-ATP, 0.3 Na-GTP (pH 7.2–7.3, ~290 mOsm/kg). We excluded recordings if series resistance or input resistance changed >20% during the recording session. We used an Axopatch 200B amplifier (Molecular Devices) and WinWCP software (J. Dempster, University of Strathclyde, Glasgow, UK) to record and collect the data, which were filtered at 10 kHz and digitized at 4–20 kHz. We collected spontaneous excitatory postsynaptic current (EPSC) data using WinEDR software (J. Dempster, University of Strathclyde) and analyzed the data using Mini Analysis (Synaptosoft, Inc., Decatur, Georgia).

DREADD characterization: We identified CeA cells adjacent to mCherry-expressing AI terminals using a scanning disk confocal microscopy (Olympus FV1000) and also used differential interference contrast optics to patch the neurons. We performed whole-cell voltage-clamp recordings ($V_{holding}$= −70mV) in visually identified neurons in CeA that were adjacent (mCherry+) or non-adjacent (mCherry-) to mCherry-expressing AI terminals. We evoked synaptic responses by stimulating axon fibers 150 μm from the recorded cell using a bipolar tungsten-stimulating electrode (140 μm tip separation, FHC). Following a 10-min

baseline period, we superfused CNO (1 mM) for 10 min. Additionally, we recorded spontaneous excitatory postsynaptic activity in each cell before and after CNO application.

TTX experiment: We performed whole cell-voltage clamp recordings ($V_{holding}= -70mV$) in visually-identified CeA neurons adjacent to eFYP-expressing AIV terminals. We evoked synaptic responses using a 473-nm laser connected to an optic fiber placed directly above the region of interest in the slice chamber. Following a 10-min baseline period we superfused TTX (1μM) for 10 min.

Statistical analyses—We analyzed the data with mixed-factorial ANOVAs, Mann-Whitney *U* tests, and Friedman tests, using the statistical program SPSS (GLM procedure). We followed significant main effects and interaction effects (p<0.05) with Bonferroni corrections to adjust for multiple comparisons. We describe the different between- and within-subjects factors for the different statistical analyses in the Results section. Because our multifactorial ANOVAs yielded multiple main and interaction effects, we only report significant effects that are critical for data interpretation. Additionally, for clarity, we indicate results of post-hoc analyses by asterisks in the figures but they are not described in the Results section. For a complete reporting of the statistical analysis, see Supplemental Table 1.

Supplementary Material

Refer to Web version on PubMed Central for supplementary material.

Acknowledgments

References

Alleweireldt AT, Hobbs RJ, Taylor AR, Neisewander JL. Effects of SCH-23390 infused into the amygdala or adjacent cortex and basal ganglia on cocaine seeking and self-administration in rats. Neuropsychopharmacology. 2006; 31:363–374. [PubMed: 15957007]

Amsel A. The role of frustrative nonreward in noncontinuous reward situations. Psychol Bull. 1958; 55:102–119. [PubMed: 13527595]

Arguello AA, Wang R, Lyons CM, Higginbotham JA, Hodges MA, Fuchs RA. Role of the agranular insular cortex in contextual control over cocaine-seeking behavior in rats. Psychopharmacology. 2017

Armbruster BN, Li X, Pausch MH, Herlitze S, Roth BL. Evolving the lock to fit the key to create a family of G protein-coupled receptors potently activated by an inert ligand. Proc Natl Acad Sci U S A. 2007; 104:5163–5168. [PubMed: 17360345]

Berglind WJ, Case JM, Parker MP, Fuchs RA, See RE. Dopamine D1 or D2 receptor antagonism within the basolateral amygdala differentially alters the acquisition of cocaine-cue associations necessary for cue-induced reinstatement of cocaine-seeking. Neuroscience. 2006; 137:699–706. [PubMed: 16289883]

Bossert JM, Stern AL, Theberge FR, Marchant NJ, Wang HL, Morales M, Shaham Y. Role of projections from ventral medial prefrontal cortex to nucleus accumbens shell in context-induced reinstatement of heroin seeking. J Neurosci. 2012; 32:4982–4991. [PubMed: 22492053]

Bossert JM, Stern AL, Theberge FRM, Cifani C, Koya E, Hope BT, Shaham Y. Ventral medial prefrontal cortex neuronal ensembles mediate context-induced relapse to heroin. Nat Neurosci. 2011; 14:420–422. [PubMed: 21336273]

Bossert JM, Wihbey K, Pickens CL, Nair SG, Shaham Y. Role of dopamine D1-family receptors in dorsolateral striatum in context-induced reinstatement of heroin seeking in rats. Psychopharmacology. 2009; 206:51–60. [PubMed: 19506837]

Cai H, Haubensak W, Anthony TE, Anderson DJ. Central amygdala PKC-delta(+) neurons mediate the influence of multiple anorexigenic signals. Nat Neurosci. 2014; 17:1240–1248. [PubMed: 25064852]

Caine SB, Koob GF. Effects of dopamine D-1 and D-2 antagonists on cocaine self-administration under different schedules of reinforcement in the rat. J Pharmacol Exp Ther. 1994; 270:209–218. [PubMed: 8035317]

Calu DJ, Chen YW, Kawa AB, Nair SG, Shaham Y. The use of the reinstatement model to study relapse to palatable food seeking during dieting. Neuropharmacology. 2014; (76 Pt B):395–406. [PubMed: 23660229]

Cantin L, Lenoir M, Augier E, Vanhille N, Dubreucq S, Serre F, Vouillac C, Ahmed SH. Cocaine is low on the value ladder of rats: possible evidence for resilience to addiction. PLoS One. 2010; 5:e11592. [PubMed: 20676364]

Caprioli D, Venniro M, Zeric T, Li X, Adhikary S, Madangopal R, Marchant NJ, Lucantonio F, Schoenbaum G, Bossert JM, Shaham Y. Effect of the novel positive allosteric modulator of metabotropic glutamate receptor 2 AZD8529 on incubation of methamphetamine craving after prolonged voluntary abstinence in a rat model. Biol Psychiatry. 2015a; 78:463–473. [PubMed: 25861699]

Caprioli D, Venniro M, Zhang M, Bossert JM, Warren BL, Hope BT, Shaham Y. Role of dorsomedial striatum neuronal ensembles in incubation of methamphetamine craving after voluntary abstinence. J Neurosci. 2017; 37:1014–1027. [PubMed: 28123032]

Caprioli D, Zeric T, Thorndike EB, Venniro M. Persistent palatable food preference in rats with a history of limited and extended access to methamphetamine self-administration. Addict Biol. 2015b; 20:913–926. [PubMed: 25582886]

Chipkin RE, Iorio LC, Coffin VL, McQuade RD, Berger JG, Barnett A. Pharmacological profile of SCH39166: a dopamine D1 selective benzonaphthazepine with potential antipsychotic activity. J Pharmacol Exp Ther. 1988; 247:1093–1102. [PubMed: 2905002]

Ciccocioppo R, Sanna PP, Weiss F. Cocaine-predictive stimulus induces drug-seeking behavior and neural activation in limbic brain regions after multiple months of abstinence: reversal by D(1) antagonists. Proc Natl Acad Sci U S A. 2001; 98:1976–1981. [PubMed: 11172061]

Cifani C, Koya E, Navarre BM, Calu DJ, Baumann MH, Marchant NJ, Liu QR, Khuc T, Pickel J, Lupica CR, et al. Medial prefrontal cortex neuronal activation and synaptic alterations after stress-induced reinstatement of palatable food seeking: a study using c-fos-GFP transgenic female rats. J Neurosci. 2012; 32:8480–8490. [PubMed: 22723688]

Ciocchi S, Herry C, Grenier F, Wolff SB, Letzkus JJ, Vlachos I, Ehrlich I, Sprengel R, Deisseroth K, Stadler MB, et al. Encoding of conditioned fear in central amygdala inhibitory circuits. Nature. 2010; 468:277–282. [PubMed: 21068837]

Cosme CV, Gutman AL, LaLumiere RT. The Dorsal agranular insular cortex regulates the cued reinstatement of cocaine-seeking, but not food-seeking, behavior in rats. Neuropsychopharmacology. 2015; 40:2425–2433. [PubMed: 25837282]

Cruz FC, Koya E, Guez-Barber DH, Bossert JM, Lupica CR, Shaham Y, Hope BT. New technologies for examining the role of neuronal ensembles in drug addiction and fear. Nat Rev Neurosci. 2013; 14:743–754. [PubMed: 24088811]

Dong Y, Nestler EJ. The neural rejuvenation hypothesis of cocaine addiction. Trends in pharmacological sciences. 2014; 35:374–383. [PubMed: 24958329]

Epstein DH, Preston KL, Stewart J, Shaham Y. Toward a model of drug relapse: an assessment of the validity of the reinstatement procedure. Psychopharmacology. 2006; 189:1–16. [PubMed: 17019567]

Erb S, Shaham Y, Stewart J. Stress-induced relapse to drug seeking in the rat: role of the bed nucleus of the stria terminalis and amygdala. Stress. 2001; 4:289–303. [PubMed: 22432148]

Feil J, Zangen A. Brain stimulation in the study and treatment of addiction. Neurosci Biobehav Rev. 2010; 34:559–574. [PubMed: 19914283]

Fuchs RA, Branham RK, See RE. Different neural substrates mediate cocaine seeking after abstinence versus extinction training: a critical role for the dorsolateral caudate-putamen. J Neurosci. 2006; 26:3584–3588. [PubMed: 16571766]

Funk D, Coen K, Tamadon S, Hope BT, Shaham Y, Le AD. Role of central amygdala neuronal ensembles in incubation of nicotine craving. J Neurosci. 2016; 36:8612–8623. [PubMed: 27535909]

Garavan H, Pankiewicz J, Bloom A, Cho JK, Sperry L, Ross TJ, Salmeron BJ, Risinger R, Kelley D, Stein EA. Cue-induced cocaine craving: neuroanatomical specificity for drug users and drug stimuli. Am J Psychiatry. 2000; 157:1789–1798. [PubMed: 11058476]

Gaznick N, Tranel D, McNutt A, Bechara A. Basal ganglia plus insula damage yields stronger disruption of smoking addiction than basal ganglia damage alone. Nicotine Tob Res. 2014; 16:445–453. [PubMed: 24169814]

Girault JA, Valjent E, Caboche J, Herve D. ERK2: a logical AND gate critical for drug-induced plasticity? Curr Opin Pharmacol. 2007; 7:77–85. [PubMed: 17085074]

Gungor NZ, Pare D. Functional heterogeneity in the bed nucleus of the stria terminalis. J Neurosci. 2016; 36:8038–8049. [PubMed: 27488624]

Harris GC, Wimmer M, Aston-Jones G. A role for lateral hypothalamic orexin neurons in reward seeking. Nature. 2005; 437:556–559. [PubMed: 16100511]

Haubensak W, Kunwar PS, Cai H, Ciocchi S, Wall NR, Ponnusamy R, Biag J, Dong HW, Deisseroth K, Callaway EM, et al. Genetic dissection of an amygdala microcircuit that gates conditioned fear. Nature. 2010; 468:270–276. [PubMed: 21068836]

Higgins ST, Heil SH, Lussier JP. Clinical implications of reinforcement as a determinant of substance use disorders. Annual review of psychology. 2004; 55:431–461.

Janak PH, Tye KM. From circuits to behaviour in the amygdala. Nature. 2015; 517:284–292. [PubMed: 25592533]

Khoo SY, Gibson GD, Prasad AA, McNally GP. How contexts promote and prevent relapse to drug seeking. Genes Brain Behav. 2017; 16:185–204. [PubMed: 27612655]

Kim J, Zhang X, Muralidhar S, LeBlanc SA, Tonegawa S. Basolateral to central amygdala neural circuits for appetitive behaviors. Neuron. 2017; 93:1464–1479. e1465. [PubMed: 28334609]

Koya E, Golden SA, Harvey BK, Guez-Barber DH, Berkow A, Simmons DE, Bossert JM, Nair SG, Uejima JL, Marin MT, et al. Targeted disruption of cocaine-activated nucleus accumbens neurons prevents context-specific sensitization. Nat Neurosci. 2009a; 12:1069–1073. [PubMed: 19620976]

Koya E, Uejima JL, Wihbey KA, Bossert JM, Hope BT, Shaham Y. Role of ventral medial prefrontal cortex in incubation of cocaine craving. Neuropharmacology. 2009b; 56(Suppl 1):177–185. [PubMed: 18565549]

Krasnova IN, Marchant NJ, Ladenheim B, McCoy MT, Panlilio LV, Bossert JM, Shaham Y, Cadet JL. Incubation of methamphetamine and palatable food craving after punishment-induced abstinence. Neuropsychopharmacology. 2014; 39:2008–2016. [PubMed: 24584329]

Kruzich PJ, See RE. Differential contributions of the basolateral and central amygdala in the acquisition and expression of conditioned relapse to cocaine-seeking behavior. J Neurosci. 2001; 21:RC155. [PubMed: 11425882]

Lee BR, Ma YY, Huang YH, Wang X, Otaka M, Ishikawa M, Neumann PA, Graziane NM, Brown TE, Suska A, et al. Maturation of silent synapses in amygdala-accumbens projection contributes to incubation of cocaine craving. Nat Neurosci. 2013; 16:1644–1651. [PubMed: 24077564]

Lenoir M, Ahmed SH. Supply of a nondrug substitute reduces escalated heroin consumption. Neuropsychopharmacology. 2008; 33:2272–2282. [PubMed: 17971831]

Lenoir M, Serre F, Cantin L, Ahmed SH. Intense sweetness surpasses cocaine reward. PLoS One. 2007; 2:e698. [PubMed: 17668074]

Li H, Penzo MA, Taniguchi H, Kopec CD, Huang ZJ, Li B. Experience-dependent modification of a central amygdala fear circuit. Nat Neurosci. 2013; 16:332–339. [PubMed: 23354330]

Li X, Rubio FJ, Zeric T, Bossert JM, Kambhampati S, Cates HM, Kennedy PJ, Liu QR, Cimbro R, Hope BT, et al. Incubation of methamphetamine craving is associated with selective increases in expression of Bdnf and trkb, glutamate receptors, and epigenetic enzymes in cue-activated fos-expressing dorsal striatal neurons. J Neurosci. 2015a; 35:8232–8244. [PubMed: 26019338]

Li X, Zeric T, Kambhampati S, Bossert JM, Shaham Y. The central amygdala nucleus is critical for incubation of methamphetamine craving. Neuropsychopharmacology. 2015b; 40:1297–1306. [PubMed: 25475163]

Lu L, Dempsey J, Shaham Y, Hope BT. Differential long-term neuroadaptations of glutamate receptors in the basolateral and central amygdala after withdrawal from cocaine self-administration in rats. J Neurochem. 2005a; 94:161–168. [PubMed: 15953359]

Lu L, Grimm JW, Dempsey J, Shaham Y. Cocaine seeking over extended withdrawal periods in rats: different time courses of responding induced by cocaine cues versus cocaine priming over the first 6 months. Psychopharmacology. 2004; 176:101–108. [PubMed: 15071719]

Lu L, Hope BT, Dempsey J, Liu SY, Bossert JM, Shaham Y. Central amygdala ERK signaling pathway is critical to incubation of cocaine craving. Nat Neurosci. 2005b; 8:212–219. [PubMed: 15657599]

Lu L, Koya E, Zhai H, Hope BT, Shaham Y. Role of ERK in cocaine addiction. Trends Neurosci. 2006; 29:695–703. [PubMed: 17084911]

Lu L, Uejima JL, Gray SM, Bossert JM, Shaham Y. Systemic and central amygdala injections of the mGluR(2/3) agonist LY379268 attenuate the expression of incubation of cocaine craving. Biol Psychiatry. 2007; 61:591–598. [PubMed: 16893525]

Luppi PH, Fort P, Jouvet M. Iontophoretic application of unconjugated cholera toxin B subunit (CTb) combined with immunohistochemistry of neurochemical substances: a method for transmitter identification of retrogradely labeled neurons. Brain Res. 1990; 534:209–224. [PubMed: 1705851]

MacLaren DA, Browne RW, Shaw JK, Krishnan Radhakrishnan S, Khare P, Espana RA, Clark SD. Clozapine N-Oxide administration produces behavioral effects in long-evans rats: implications for designing DREADD experiments. eNeuro. 2016:3.

Mahler SV, Vazey EM, Beckley JT, Keistler CR, McGlinchey EM, Kaufling J, Wilson SP, Deisseroth K, Woodward JJ, Aston-Jones G. Designer receptors show role for ventral pallidum input to ventral tegmental area in cocaine seeking. Nat Neurosci. 2014; 17:577–585. [PubMed: 24584054]

Mantsch JR, Baker DA, Funk D, Le AD, Shaham Y. Stress-induced reinstatement of drug seeking: 20 years of progress. Neuropsychopharmacology. 2016; 41:335–356. [PubMed: 25976297]

Marchant NJ, Campbell EJ, Whitaker LR, Harvey BK, Kaganovsky K, Adhikary S, Hope BT, Heins RC, Prisinzano TE, Vardy E, et al. Role of ventral subiculum in context-induced relapse to alcohol seeking after punishment-imposed abstinence. J Neurosci. 2016; 36:3281–3294. [PubMed: 26985037]

Marchant NJ, Hamlin AS, McNally GP. Lateral hypothalamus is required for context-induced reinstatement of extinguished reward seeking. J Neurosci. 2009; 29:1331–1342. [PubMed: 19193880]

Marchant NJ, Li X, Shaham Y. Recent developments in animal models of drug relapse. Curr Opin Neurobiol. 2013; 23:675–683. [PubMed: 23374536]

Marchant NJ, Rabei R, Kaganovsky K, Caprioli D, Bossert JM, Bonci A, Shaham Y. A critical role of lateral hypothalamus in context-induced relapse to alcohol seeking after punishment-imposed abstinence. J Neurosci. 2014; 34:7447–7457. [PubMed: 24872550]

McFarland K, Kalivas PW. The circuitry mediating cocaine-induced reinstatement of drug-seeking behavior. J Neurosci. 2001; 21:8655–8663. [PubMed: 11606653]

McLaughlin J, See RE. Selective inactivation of the dorsomedial prefrontal cortex and the basolateral amygdala attenuates conditioned-cued reinstatement of extinguished cocaine-seeking behavior in rats. Psychopharmacology. 2003; 168:57–65. [PubMed: 12845418]

Micioni Di Bonaventura MV, Ciccocioppo R, Romano A, Bossert JM, Rice KC, Ubaldi M, St Laurent R, Gaetani S, Massi M, Shaham Y, Cifani C. Role of bed nucleus of the stria terminalis corticotrophin-releasing factor receptors in frustration stress-induced binge-like palatable food consumption in female rats with a history of food restriction. J Neurosci. 2014; 34:11316–11324. [PubMed: 25143612]

Morgan JI, Curran T. Stimulus-transcription coupling in the nervous system: involvement of the inducible proto-oncogenes fos and jun. Annu Rev Neurosci. 1991; 14:421–451. [PubMed: 1903243]

Naqvi NH, Rudrauf D, Damasio H, Bechara A. Damage to the insula disrupts addiction to cigarette smoking. Science. 2007; 315:531–534. [PubMed: 17255515]

Pelloux Y, Murray JE, Everitt BJ. Differential roles of the prefrontal cortical subregions and basolateral amygdala in compulsive cocaine seeking and relapse after voluntary abstinence in rats. Eur J Neurosci. 2013; 38:3018–3026. [PubMed: 23815783]

Penzo MA, Robert V, Li B. Fear conditioning potentiates synaptic transmission onto long-range projection neurons in the lateral subdivision of central amygdala. J Neurosci. 2014; 34:2432–2437. [PubMed 24523533]

Pickens CL, Airavaara M, Theberge F, Fanous S, Hope BT, Shaham Y. Neurobiology of the incubation of drug craving. Trends Neurosci. 2011; 34:411–420. [PubMed: 21764143]

Pickens CL, Cifani C, Navarre BM, Eichenbaum H, Theberge FR, Baumann MH, Calu DJ, Shaham Y. Effect of fenfluramine on reinstatement of food seeking in female and male rats: implications for the predictive validity of the reinstatement model. Psychopharmacology. 2012; 221:341–353. [PubMed: 22134478]

Pitkanen, A. Connectivity of the rat amygaloid complex. In: Aggleton, JP., editor. The amygdala: a functional analysis. Oxford: Oxford University Press; 2000. p. 31-115.

Pushparaj A, Kim AS, Musiol M, Trigo JM, Le Foll B. Involvement of the rostral agranular insular cortex in nicotine self-administration in rats. Behav Brain Res. 2015; 290:77–83. [PubMed: 25934486]

Robertson GS, Jian M. D1 and D2 dopamine receptors differentially increase Fos-like immunoreactivity in accumbal projections to the ventral pallidum and midbrain. Neuroscience. 1995; 64:1019–1034. [PubMed: 7753373]

Rocha A, Kalivas PW. Role of the prefrontal cortex and nucleus accumbens in reinstating methamphetamine seeking. Eur J Neurosci. 2010; 31:903–909. [PubMed: 20180839]

Roll JM. Contingency management: an evidence-based component of methamphetamine use disorder treatments. Addiction. 2007; 102(Suppl 1):114–120.

Rotge JY, Cocker PJ, Daniel ML, Belin-Rauscent A, Everitt BJ, Belin D. Bidirectional regulation over the development and expression of loss of control over cocaine intake by the anterior insula. Psychopharmacology. 2017

Rubio FJ, Liu QR, Li X, Cruz FC, Leao RM, Warren BL, Kambhampati S, Babin KR, McPherson KB, Cimbro R, et al. Context-induced reinstatement of methamphetamine seeking is associated with unique molecular alterations in Fos-expressing dorsolateral striatum neurons. J Neurosci. 2015; 35:5625–5639. [PubMed: 25855177]

Sakanaka M, Shibasaki T, Lederis K. Distribution and efferent projections of corticotropin-releasing factor-like immunoreactivity in the rat amygdaloid complex. Brain Res. 1986; 382:213–238. [PubMed: 2428439]

See RE, Kruzich PJ, Grimm JW. Dopamine, but not glutamate, receptor blockade in the basolateral amygdala attenuates conditioned reward in a rat model of relapse to cocaine-seeking behavior. Psychopharmacology. 2001; 154:301–310. [PubMed: 11351937]

Seif T, Chang SJ, Simms JA, Gibb SL, Dadgar J, Chen BT, Harvey BK, Ron D, Messing RO, Bonci A, Hopf FW. Cortical activation of accumbens hyperpolarization-active NMDARs mediates aversion-resistant alcohol intake. Nat Neurosci. 2013; 16:1094–1100. [PubMed: 23817545]

Shalev U, Grimm JW, Shaham Y. Neurobiology of relapse to heroin and cocaine seeking: a review. Pharmacol Rev. 2002; 54:1–42. [PubMed: 11870259]

Shi CJ, Cassell MD. Cortical, thalamic, and amygdaloid connections of the anterior and posterior insular cortices. J Comp Neurol. 1998; 399:440–468. [PubMed: 9741477]

Stewart J, de Wit H, Eikelboom R. Role of unconditioned and conditioned drug effects in the self-administration of opiates and stimulants. Psychological review. 1984; 91:251–268. [PubMed: 6571424]

Stopper CM, Floresco SB. What's better for me? Fundamental role for lateral habenula in promoting subjective decision biases. Nat Neurosci. 2014; 17:33–35. [PubMed: 24270185]

Theberge FR, Li X, Kambhampati S, Pickens CL, St Laurent R, Bossert JM, Baumann MH, Hutchinson MR, Rice KC, Watkins LR, Shaham Y. Effect of chronic delivery of the Toll-like receptor 4 antagonist (+)-naltrexone on incubation of heroin craving. Biol Psychiatry. 2013; 73:729–737. [PubMed: 23384483]

Tovote P, Esposito MS, Botta P, Chaudun F, Fadok JP, Markovic M, Wolff SB, Ramakrishnan C, Fenno L, Deisseroth K, et al. Midbrain circuits for defensive behaviour. Nature. 2016; 534:206–212. [PubMed: 27279213]

Venniro M, Caprioli D, Shaham Y. Animal models of drug relapse and craving: From drug priming-induced reinstatement to incubation of craving after voluntary abstinence. Prog Brain Res. 2016; 224:25–52. [PubMed: 26822352]

Venniro M, Zhang M, Shaham Y, Caprioli D. Incubation of methamphetamine but not heroin craving after voluntary abstinence in male and female rats. Neuropsychopharmacology. 2017; 42:1126–1135. [PubMed: 28025975]

Wang F, Flanagan J, Su N, Wang LC, Bui S, Nielson A, Wu X, Vo HT, Ma XJ, Luo Y. RNAscope: a novel in situ RNA analysis platform for formalin-fixed, paraffin-embedded tissues. J Mol Diagn. 2012; 14:22–29. [PubMed: 22166544]

Warren BL, Mendoza MP, Cruz FC, Leao RM, Caprioli D, Rubio FJ, Whitaker LR, McPherson KB, Bossert JM, Shaham Y, Hope BT. Distinct fos-expressing neuronal ensembles in the ventromedial prefrontal cortex mediate food reward and extinction memories. J Neurosci. 2016; 36:6691–6703. [PubMed: 27335401]

Weiss F, Martin-Fardon R, Ciccocioppo R, Kerr TM, Smith DL, Ben-Shahar O. Enduring resistance to extinction of cocaine-seeking behavior induced by drug-related cues. Neuropsychopharmacology. 2001; 25:361–372. [PubMed: 11522464]

Wise RA. Addictive drugs and brain stimulation reward. Annu Rev Neurosci. 1996; 19:319–340. [PubMed: 8833446]

Wolf ME. Synaptic mechanisms underlying persistent cocaine craving. Nat Rev Neurosci. 2016; 17:351–365. [PubMed: 27150400]

Wright CI, Groenewegen HJ. Patterns of overlap and segregation between insular cortical, intermediodorsal thalamic and basal amygdaloid afferents in the nucleus accumbens of the rat. Neuroscience. 1996; 73:359–373. [PubMed: 8783254]

Xi ZX, Li X, Li J, Peng XQ, Song R, Gaal J, Gardner EL. Blockade of dopamine D3 receptors in the nucleus accumbens and central amygdala inhibits incubation of cocaine craving in rats. Addict Biol. 2013; 18:665–677. [PubMed: 22913325]

Yin JJ, Ma SH, Xu K, Wang ZX, Le HB, Huang JZ, Fang KM, Liao LM, Cai ZL. Functional magnetic resonance imaging of methamphetamine craving. Clin Imaging. 2012; 36:695–701. [PubMed: 23153997]

Zhang S, Qi J, Li X, Wang HL, Britt JP, Hoffman AF, Bonci A, Lupica CR, Morales M. Dopaminergic and glutamatergic microdomains in a subset of rodent mesoaccumbens axons. Nat Neurosci. 2015; 18:386–392. [PubMed: 25664911]

Highlights

- CeA activity is critical to drug relapse after choice-based contingency management

- Relapse is associated with selective activation of AIV→CeA glutamatergic projection

- AIV activity is critical to drug relapse after contingency management

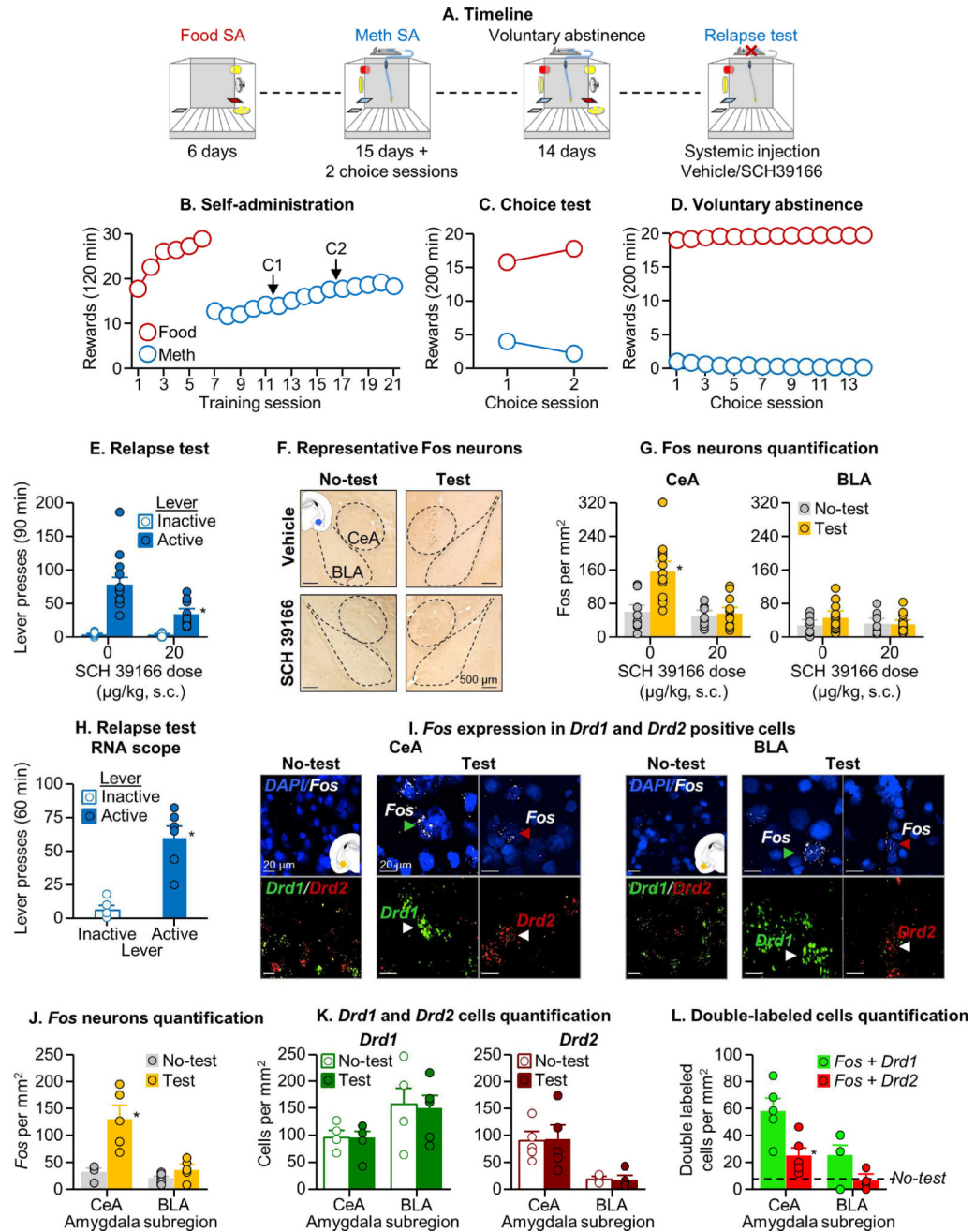- Chemogenetic inhibition of the monosynaptic AIV→CeA projection decreased relapse

Figure 1. Systemic Drd1 antagonist injections decreased relapse after voluntary abstinence and relapse-induced activation of CeA

(**A**) Timeline of the experiment. The operant chamber is equipped with two active levers (drug and food), one inactive lever, two discriminative cues (red light for drug and yellow light for food), two conditioned stimuli (white light for drug and tone for food), a pump, and a food receptacle. (**B**) Self-administration training: Number of food rewards (5 palatable food pellets/reward delivery) or methamphetamine infusions (0.1 mg/kg/infusion) during the 120-min sessions (total n=54). (**C**) Discrete choice sessions during training: Food rewards and methamphetamine infusions earned during the 2 discrete choice sessions that were

performed during training (20 trials every 10 min). (**D**) <u>Voluntary abstinence</u>: Number of food rewards and methamphetamine infusions earned during the 14 discrete choice sessions. (**E**) <u>Relapse test</u>: Lever presses on the active and inactive levers during the 90-min test session. During testing, active lever presses led to contingent presentations of the light cue previously paired with methamphetamine infusions during training, but not methamphetamine infusions (extinction conditions). We injected vehicle or SCH39166 (20 μg/kg, s.c) 30 min before testing (n=13–14 per group). The No-test group was kept undisturbed in their home cage (n=8 per group). * Different from the active lever in the vehicle condition, p<0.05 (**F**) Representative photomicrographs of Fos cells in central (CeA) and basolateral (BLA) amygdala. (**G**) <u>Amygdala c-Fos expression</u>: Number of *Fos*-IR nuclei per mm^2 in the CeA and BLA. * Different from the No-test group, p<0.05 (**H**) <u>Relapse test RNAscope</u>: Lever presses on the active and inactive levers during the 60-min test sessions (n=5–6 per group). * Different from inactive lever, p<0.05 (**I**) Representative photomicrographs of CeA and BLA and *Fos* labelling in the Relapse test and No-test groups, and *Drd1* or *Drd2* labelling in the Relapse test group (*Fos*, white; *Drd1*, green; *Drd2*, red; DAPI, blue). Arrows indicate representative cells. (**J**) <u>*Fos*-IR neurons</u>: Number of *Fos*-IR nuclei per mm^2 in CeA and BLA. * Different from the No-test group, p<0.05 (**K**) <u>*Drd1* and *Drd2* positive cells</u>: Number of *Drd1* and *Drd2* cells in CeA and BLA. * Different from the No-test group, p<0.05 (**L**) <u>*Fos*-IR co-expression with *Drd1* or *Drd2*</u>: Number of double-labeled neurons per mm^2 in the CeA and BLA. * Different from *Fos+Drd1*, p<0.05. Data are mean±SEM. See also Figure S1 and S2.
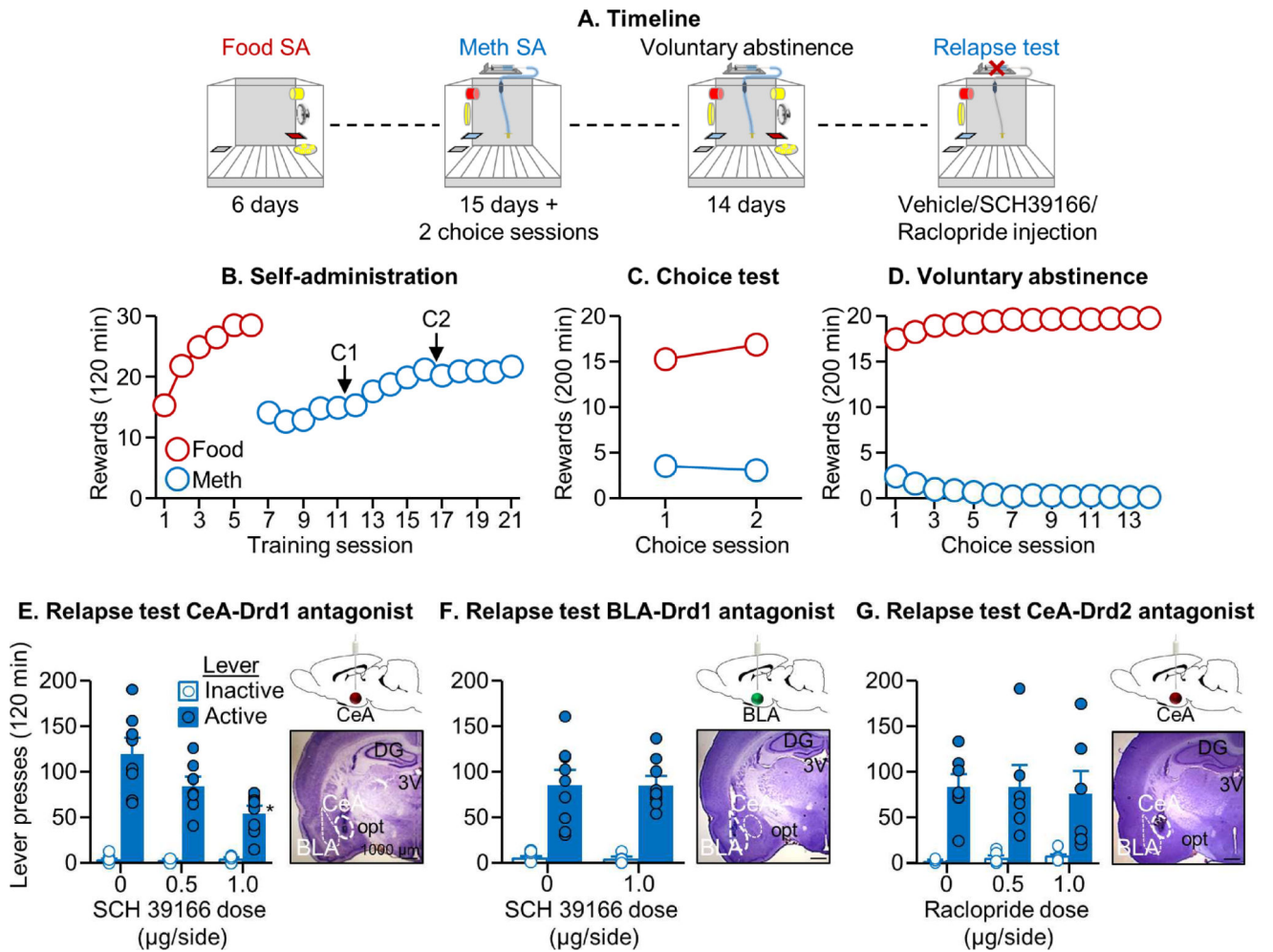
Figure 2. CeA Drd1 antagonist injections decreased relapse after voluntary abstinence

(**A**) Timeline of the experiment. (**B**) <u>Self-administration training</u>: Number of food rewards or methamphetamine infusions during the 120-min sessions (total n=61). (**C**) <u>Discrete choice sessions during training</u>: Food rewards and methamphetamine infusions earned during the 2 discrete choice sessions that were performed during training. (**D**) <u>Voluntary abstinence</u>: Number of food rewards and methamphetamine infusions earned during the 14 discrete choice sessions. (**E, F, G**) <u>Relapse test</u>: Lever presses on the active and inactive levers during the 2-h test sessions. We injected vehicle or SCH39166 (in CeA and BLA; 0.5, 1.0 µg/side) or raclopride (in CeA; 0.5, 1.0 µg/side) 15 min before the test sessions (n=7–9 per group). For each experiment, we added a representative photomicrograph of the cannula placement in CeA or BLA (scale=1000 µm). * Different from the active lever in the vehicle condition, p<0.05. Data are mean±SEM. See also Figure S1 and S3.
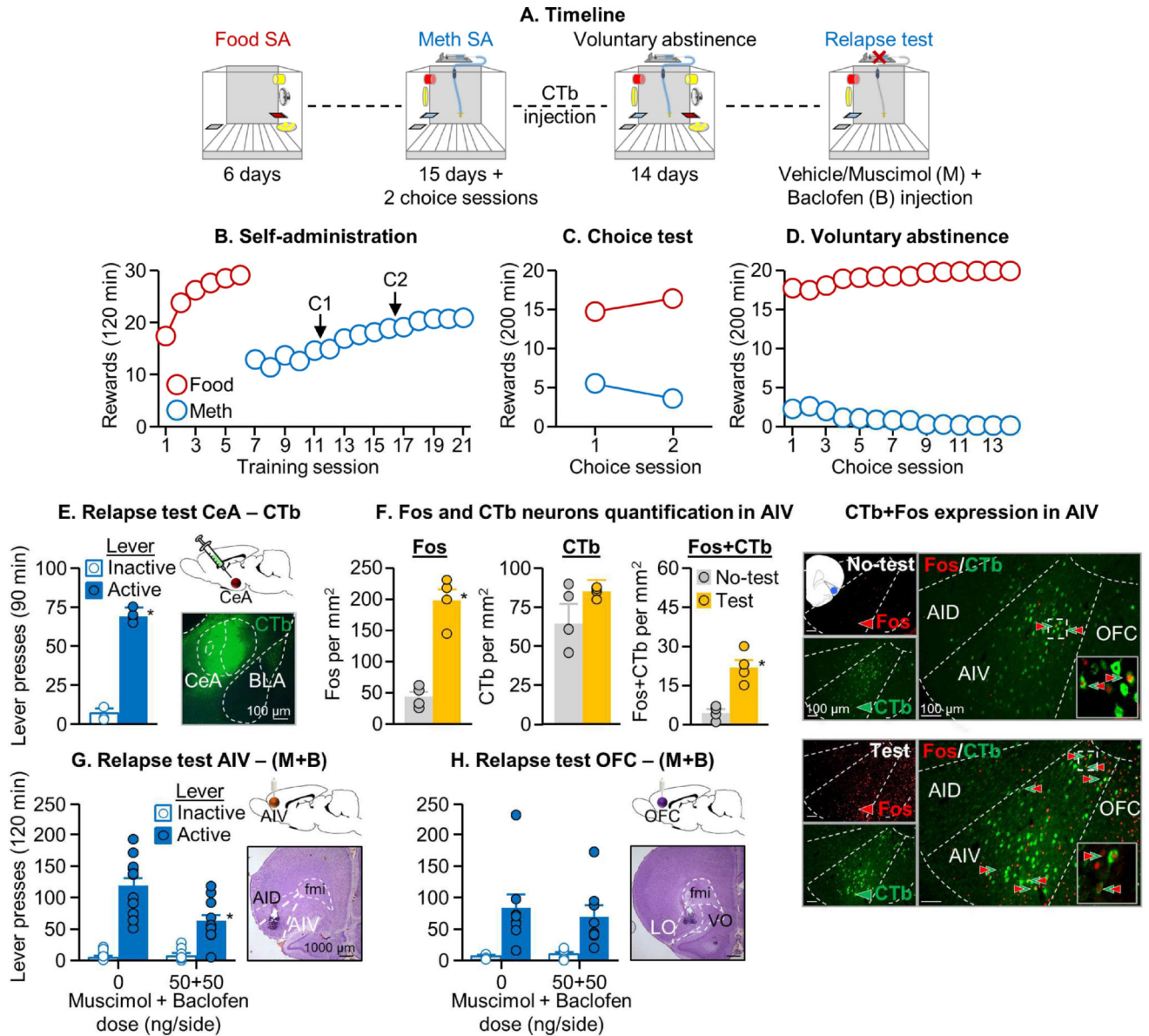
Figure 3. Relapse after voluntary abstinence is associated with selective activation of the AIV→CeA projection and inhibition of neuronal activity in AIV decreased relapse after voluntary abstinence

(**A**) Timeline of the experiment (total n=46). (**B**) Self-administration training: Number of food rewards or methamphetamine infusions during the 120-min sessions. (**C**) Discrete choice sessions during training: Food rewards and methamphetamine infusions earned during the 2 discrete choice sessions that were performed during training. (**D**) Voluntary abstinence: Number of food rewards and methamphetamine infusions earned during the discrete choice sessions. (**E**) Relapse test for CTb injections: Lever presses on the active and inactive levers the 90-min test session and a representative photomicrograph of CeA CTb expression (n=4 per group). * Different from the vehicle condition, p<0.05 (**F**) Fos and CTb expression in the AIV: number of Fos-IR, CTb-IR, and CTb+Fos-IR double-labeled neurons per mm² of either test or no test rats (n=4 per group) in the AIV. Representative

photomicrograph of a CTb injection into CeA (scale=100 μm). **Green arrows**=CTb-IR neurons, **Red arrows**=Fos-IR neurons, **Green+Red** arrows=double-labeled neurons. * Different from the No-test group, p<0.05. (**G-H**) <u>Relapse test for M+B injections—AIV and OFC</u>: Lever presses on the active and inactive levers during the 2-h test session. We injected vehicle or M+B (50 ng+50 ng/side) into the AIV or OFC 15 min before the test session (n=8–12 per group). We added a representative photomicrograph of the cannula placement in AIV and OFC (scale=1000 μm). * Different from the vehicle condition, p<0.05. Data are mean±SEM. See also Figure S1, S3, S4 and S5.
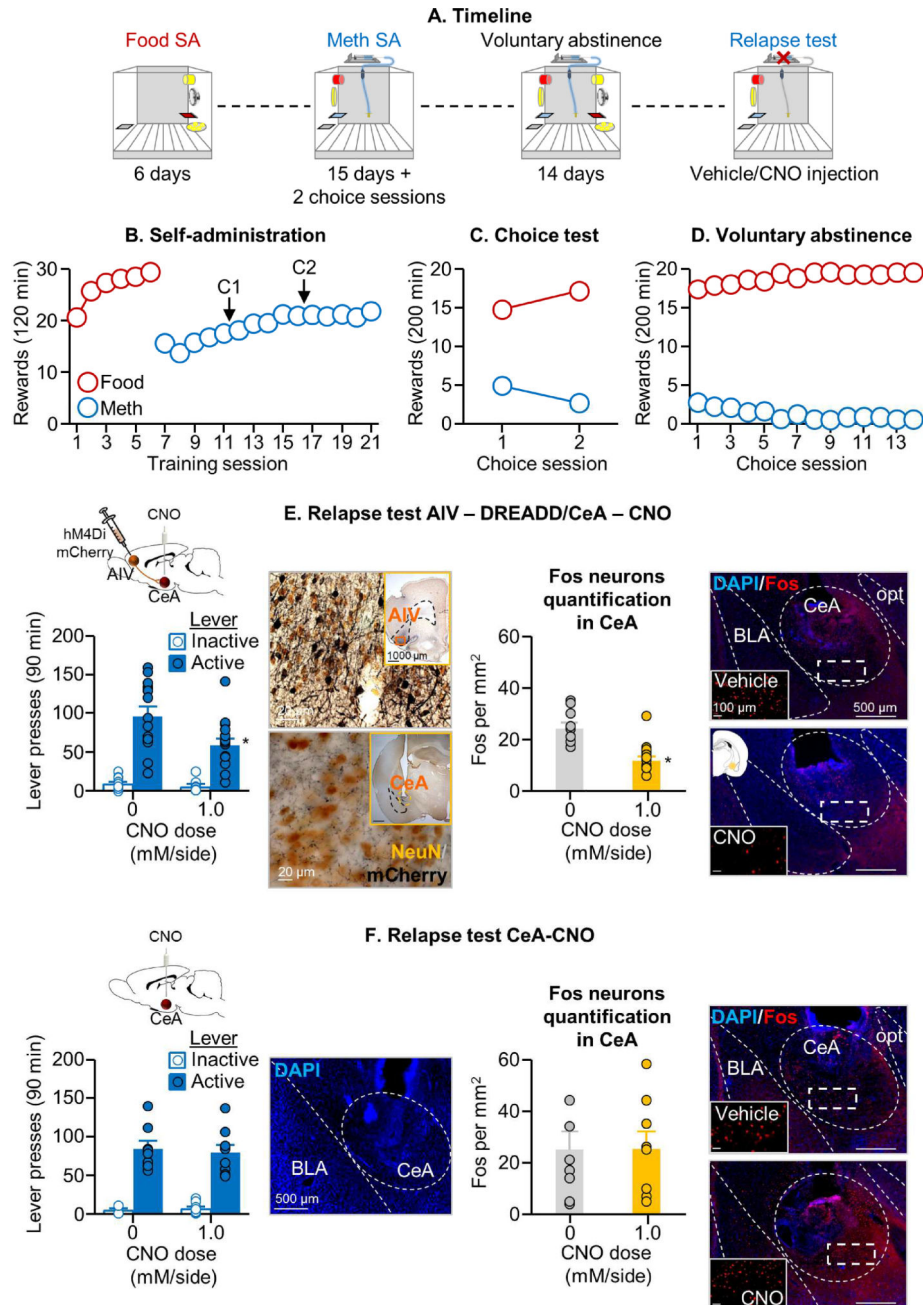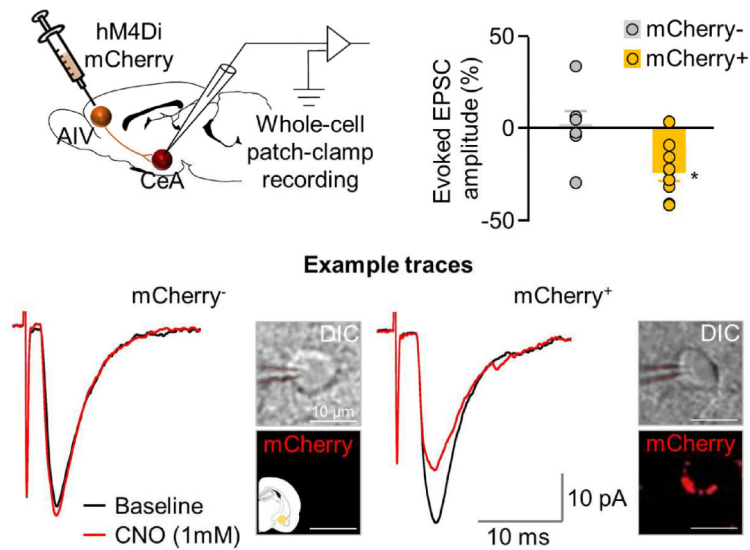
Figure 4. Inhibition of neuronal activity in AIV→CeA projection decreased relapse after voluntary abstinence

(**A**) Timeline of the experiment. (**B**) Self-administration training: Number of food rewards or methamphetamine infusions during the 120-min sessions (total n=47). (**C**) Discrete choice sessions during training: Food rewards and methamphetamine infusions earned during the 2 discrete choice sessions that were performed during training. (**D**) Voluntary abstinence: Number of food rewards and methamphetamine infusions earned during the discrete choice sessions. (**E**) Relapse test with DREADD injection. Left: Lever presses on the active and inactive levers during the 90-min extinction session (n=15 per group). We injected vehicle or CNO (1.0 mM/0.5 μL/side) 30 min before the test session. We include a representative

micrograph of NeuN + mCherry double labeling immunohistochemistry in the AIV (cell bodies) and CeA (terminals) (scale=20 μm). Insertions represent virus in AIV and CeA cannula placement (scale=1000 μm). * Different from the active lever in the vehicle condition, p<0.05. <u>Right</u>: Number of Fos-IR positive cell per mm^2 in the CeA after vehicle or CNO. We include a representative photomicrograph of cannula placement in CeA for each CNO dose (scale=500 μm). Magnifications represent Fos expression for each CNO dose (scale=100 μm). * Different from the vehicle condition, p<0.05. (**F**) <u>Relapse test without DREADD injection, Left</u>: Lever presses on the active and inactive levers during the 90-min test session (n=8–9 per group). We injected vehicle or CNO (1.0 mM/0.5 μL/side) 30 min before the test sessions. We added a representative photomicrograph of the cannula placement in CeA (scale=500 μm). <u>Right</u>: Number of Fos-IR positive cell per mm^2 in the CeA after vehicle or CNO. Representative photomicrograph of cannula placement in CeA for each CNO dose (scale=500 μm). Magnifications represent Fos expression for each CNO dose (scale=100 μm). * Different from the vehicle condition, p<0.05.
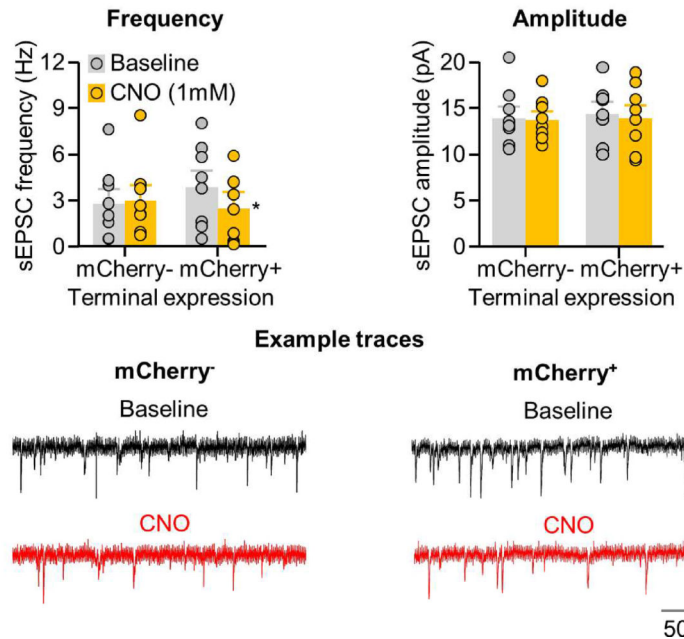
Figure 5. Effect of CNO application on evoked and spontaneous EPSC in rats expressing hM4Di receptors in AIV→CeA neurons

(**A**) <u>Top right</u>: A summary graph demonstrating percent change in evoked EPSC amplitude in CeA neurons following bath application of CNO onto AIV terminals expressing (mCherry +) or not expressing (mCherry-) hM4Di receptors (n=6). <u>Bottom</u>: Example traces from recorded mCherry+ (n=9) and mCherry- (n=7) CeA neurons following bath application of CNO. Representative photomicrograph of recorded cells (scale=10 μm). (**B**) <u>Spontaneous EPSC in CeA</u>. <u>Top left</u>: Summary graph showing spontaneous event frequency; <u>Top right</u>: spontaneous event amplitude, before and after CNO application in mCherry+ and mCherry CeA neurons; <u>Bottom</u>: Spontaneous event example traces from mCherry+ and mCherry-

CeA neurons before and after CNO application (n=8 mCherry+, and n=7 mCherry- cells from 6 rats).

A. AIV-terminals express vGluT1 in CeA

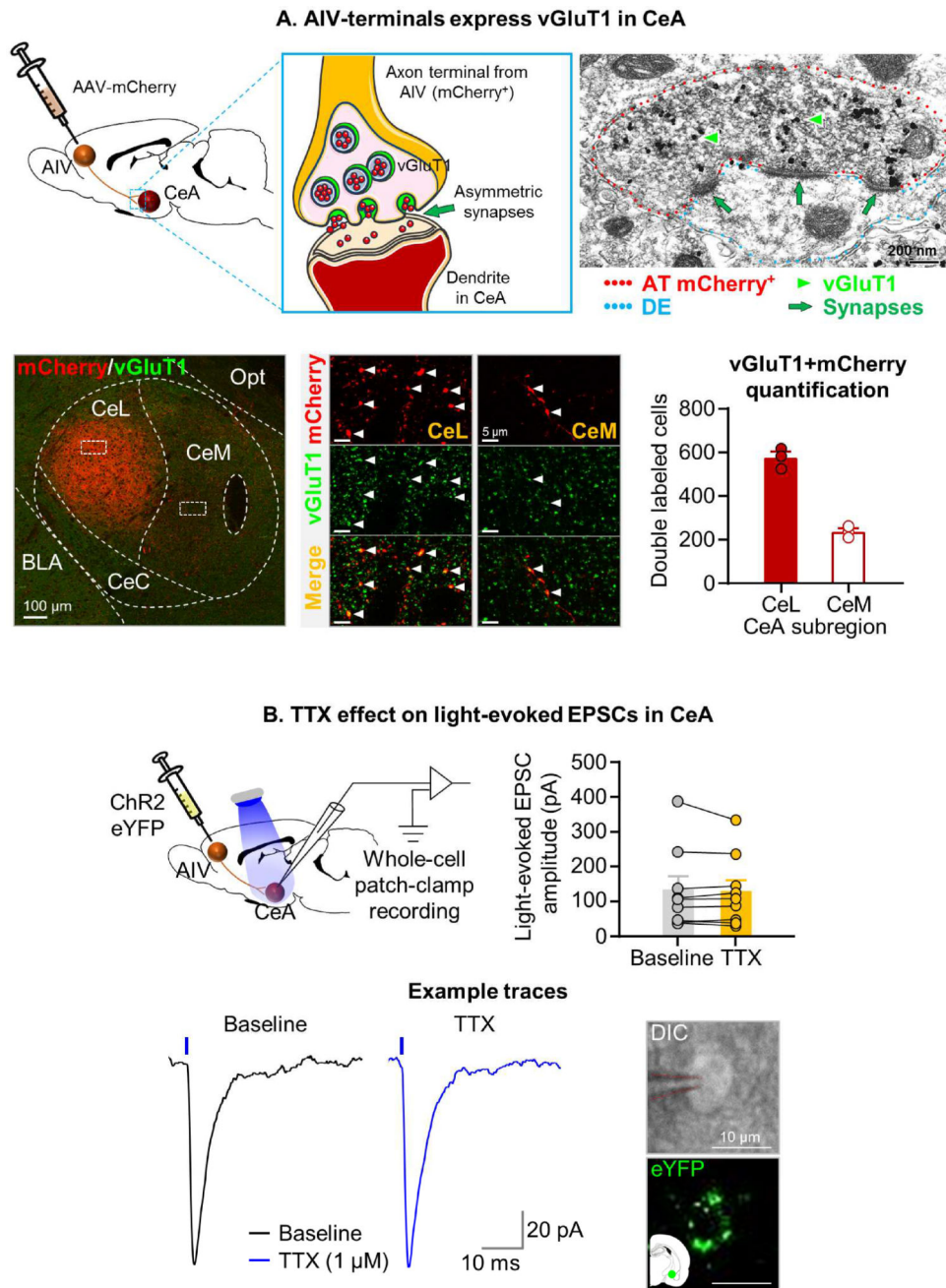## B. TTX effect on light-evoked EPSCs in CeA

Figure 6. (A) AIV vGluT1 projection neurons make asymmetric synapses on CeA cell bodies
Top left: Schemes of viral (AAV-mCherry) injection within the AIV for the tagging of neurons, and characterization of their inputs within the CeA, which co-expressed mCherry and vGluT1 immunoreactivity and make asymmetric synapses onto dendrites (top center). Top right: An axon terminal (AT) (**red outline**) from an AIV neuron co-expressing mCherry (scattered dark material) and vGluT1 (**gold** particles, **green** arrowheads), which is making three asymmetric synapses (**green** arrows) onto a dendrite in the CeA (De, **blue outline**) (scale=200 nm) (n=3). Bottom Left: CeL and CeM detection of AAV fibers containing mCherry (**red**) (scale = 100 μm). Bottom center: CeL and CeM delimited areas

by white boxes (bottom left) are seen at high magnification showing terminal-like puncta co-expressing mCherry and vGluT1 (white arrowheads) (scale = 5 μm). <u>Bottom right</u>: 3-D quantification of axon terminals showing that AAV fibers containing mCherry and vGluT1 primarily innervate the CeL. Data are mean±SEM. (**B**) *TTX has no effect on light-evoked EPSCs in CeA*. <u>Top left</u>: Schematic representation of recording configuration. We recorded from CeA neurons visually contacted by eYFP-expressing terminals. <u>Top right</u>: Summary graph showing no significant effect of TTX bath application on light-evoked EPSCs in CeA. <u>Bottom left</u>: Example traces of light-evoked EPSCs in CeA neurons before and after application of TTX. <u>Bottom right</u>: Representative micrograph of recorded cells (scale=10 μm).

Key resources table

Further information and requests for resources and reagents should be directed to and will be fulfilled by the Lead Contact Yavin Shaham (Yshaham@intra.nida.nih.gov)

Reagent	Source	Identifier
Antibodies		
Rabbit anti-c-Fos primary antibody	Cell Signaling Technology Phospho-c-Fos, 5348S,	AB_10557109
Goat anti-CTb primary antibody	List Biological Laboratories CTb 703	AB_10013220
Mouse anti-mCherry primary antibody	Clontech Laboratories 632543	AB_2307319
Mouse anti-NeuN primary antibody	Millipore MAB377	AB_2298772
Biotinylated anti-rabbit IgG secondary antibody	Vector Laboratories	BA-1000
Donkey anti-goat Alexa Fluor 488	Jackson ImmunoResearch, 705-546-147	AB_2340430
Donkey anti-rabbit Alexa Fluor 594	Jackson ImmunoResearch 711-585-152	AB_2340621
Biotinylated anti-mouse IgG secondary antibody	Vector Laboratories	BA-9200
Critical Commercial Assays		
Avidin-biotin-peroxidase complex ABC Elite kit	Vector Laboratories	PK-6100
RNAscope Multiplex Fluorescent Reagent Kit	Advanced Cell Diagnostics	Cat# 320851
Experimental Models: Organisms/Strains		
Sprague-Dawley rats	Charles River	
Drugs		
Methamphetamine	NIDA	
SCH39166	Tocris Bioscience	Cat# 2299
Raclopride	Sigma Aldrich	Cat# 98185-20-7
Muscimol	Tocris Bioscience	Cat# 0289
Baclofen	Tocris Bioscience	Cat# 0417
CNO	Tocris Bioscience	Cat# 4936
Tetrodotoxin (TTX)	Tocris Bioscience	Cat# 1078
4-Aminopyridine (4 AP)	Tocris Bioscience	Cat# 0940
Retrograde traces and Viruses		
CTb	List Biological Laboratories	Cat# 703
AAV8-hSynp-hM4Di-mCherry	UNC vector core	Lot# AV5360D
AAV5-CaMKIIa-hChR2 (E123T/T159C)-EYFP	UNC vector core	Lot# AV4824
Sequence-Based Reagents		
RNAscope Probe Drd1a	Advanced Cell Diagnostics	Cat# 317031
RNAscope Probe Drd2	Advanced Cell Diagnostics	Cat# 315641-C2
RNAscope Probe Fos	Advanced Cell Diagnostics	Cat# 403591-C3
Software		
iVision (4.0.15 and 4.5.0)	Biovision Technologies	
ImageJ	https://imagej.net/Fiji/Downloads	
MED-PC	Med-associates	